FULL PAPER

Open Access

Geomagnetic and ionospheric response to the interplanetary shock on January 24, 2012

V. B. Belakhovsky[1], V. A. Pilipenko[2*], Ya. A. Sakharov[3], D. L. Lorentzen[4,5] and S. N. Samsonov[6]

Abstract

We have examined multi-instrument observations of the magnetospheric and ionospheric response to the interplanetary shock on January 24, 2012. Apart from various instruments, such as ground and space magnetometers, photometers, and riometers used earlier for a study of possible response to a shock, we have additionally examined variations of the ionospheric total electron content as determined from the global navigation satellite system receivers. Worldwide ground magnetometer arrays detected shock-induced sudden commencement (SC) with preliminary and main impulses throughout the dayside sector. A magnetic field compression was found to propagate through the magnetosphere with velocity less than the local Alfven velocity. Though the preliminary pulse was evident on the ground, its signature was not observed by the THEMIS and GOES satellites in the magnetosphere. The SC was accompanied by a burst of cosmic noise absorption recorded along a latitudinal network of riometers in the morning and evening sectors. The SC also caused an impulsive enhancement of dayside auroral emissions (shock aurora) as observed by the hyperspectral all-sky imager NORUSCA II at Barentsburg and the meridian scanning photometer at Longyearbyen (both at Svalbard). The VHF EISCAT radar (Tromsø, Norway) observed a SC-associated increase in electron density in the lower ionosphere (100–180 km). The system for monitoring geomagnetically induced currents (GICs) in power lines at the Kola Peninsula recorded a burst of GIC during the SC. A $\leq$10% positive pulse of the ionospheric total electron content caused by the SC in the dusk sector was found. On the basis of the multi-instrument information, a validated theory of the magnetosphere–ionosphere response to IP shock may be constructed.

Keywords: Storm commencement, Magnetometers, Riometers, GPS/TEC technique, EISCAT radar, Dayside shock aurora

Introduction

An impact of interplanetary (IP) shock or tangential discontinuity onto the magnetosphere, observed by ground magnetometers as storm sudden commencement (SC), is a convenient probing signal for the experimental study of near-Earth space. Most SC events are associated with IP shocks (Smith et al. 1986), and, therefore, we will use both terms interchangeably. During a relatively short time period (<10 min), significant energy and momentum is pumped into the magnetosphere from the solar wind. Modelers often use a SC event to validate the numerical models of the solar wind–magnetosphere–ionosphere interaction (Fujita et al. 2003; Sun et al. 2015). Despite the

simplicity of such an impact, the complexity of impulsive and quasiperiodic phenomena stimulated by an IP shock in the ultra-low-frequency (ULF) band (timescales from few seconds to tens of minutes) turns out to be surprisingly large. An observed response to an IP shock or discontinuity may be rather complicated due to the nearly simultaneous excitation of several transient processes. The IP shock is known to stimulate a global compression of the magnetosphere (Araki 1994), with excitation of transient field-aligned current systems (Fujita et al. 2005), generation of transient ULF waves in a wide frequency band from Pc1 (Parkhomov 1990) to Pc5–6 (Yumoto et al. 1994), triggering of VLF wave activity and enhancement of energetic electron precipitation (Gail et al. 1990), brightening of the dayside aurora ("shock aurora") at auroral (Spann et al. 1998; Vorobiev et al. 2008) and sub-auroral (Liou et al. 2003) latitudes, sudden vertical

*Correspondence: space.soliton@gmail.com
[2] Geophysical Center, Moscow, Russia
Full list of author information is available at the end of the article

Belakhovsky *et al. Earth, Planets and Space* (2017) 69:105

Page 2 of 25

shifting of the ionospheric plasma (Yumoto et al. 1989), prompt injection and energization up to MeV energies of magnetospheric particles (Blake et al. 1992), and triggering of a nightside "compression" magnetic bay or even a substorm (Lyons 1996; Liou et al. 2003). In addition, a SC pulse serves as an indicator of the onset of a more intense solar wind driving and buffeting the magnetosphere.

Though the basic physics of the related phenomena is qualitatively understood, some aspects of the IP shock impact on the magnetosphere–ionosphere system have not been sufficiently established. Based on the analysis of ground magnetometer data, Araki (1994) suggested a phenomenological model of SC, in which an observed disturbance is interpreted as the superposition of a stepwise compression of the geomagnetic field (DL component) and bipolar impulse, composed of a short preliminary impulse (PI) followed by a main impulse (MI). The nature of a stepwise increase in the geomagnetic field (DL) is now clearly identified as a result of global compression of the magnetosphere. The MI and PI are supposedly associated with transient magnetospheric field-aligned current (FAC) systems driven by different mechanisms. The sequential occurrence of two transient FAC systems in the magnetosphere produces large-scale ionospheric vortex-like current systems on the morning and evening sides. The MI vortex is clockwise/anticlockwise driven by the FAC flowing into/out of the ionosphere on the dawn/duskside, while the PI vortex has an opposite polarity. The PI currents are supposed to be related to inertial currents of a compressional wave propagating through the magnetosphere, while the MI currents are associated with diamagnetic currents of tailward-propagating pressure structures along the magnetopause.

The magnetospheric cusp is the first region to directly respond to IP shocks in geospace, so detailed studies focusing on the shock-related phenomena around the dayside cusp are essential in revealing the physics of its early response. Dayside auroras observed right after the impingement of solar wind pressure pulses or IP shocks, referred to as "shock aurora," exhibit some features that are different from typical auroral activity. Auroral behaviors were suggested to differ during PI and MI, indicating that these differences can be used potentially as optical counterparts of SC-related FACs (Motoba et al. 2009). Initial brightening of shock aurora usually occurs near the ionospheric footprint of the dayside cusp and propagates toward dawnside and duskside along the auroral oval with speeds of several km/s (Holmes et al. 2014). In the afternoon sector, the auroral counterpart of the PI was attributed to mainly proton precipitation, while the MI observed shortly thereafter was assumed to be accompanied by both proton and electron precipitation

(Motoba et al. 2009). The PI was related to diffuse auroral brightening that occur several degrees equatorward of the preexisting discrete aurora, while the MI was associated with the discrete auroral brightening poleward of the diffuse aurora (Nishimura et al. 2016).

Because of multiple aspects of the IP shock impact on the magnetosphere and ionosphere, any comprehensive description can be achieved only with the use of multiple instruments, both in space and on the ground. Magnetometers, riometers, optical imagers, satellite particle detectors, and ionospheric radars have become a standard tool for monitoring the solar wind–magnetosphere–ionosphere coupling. For an examination of the ionospheric response to solar wind pressure pulses, Jayachandran et al. (2011) suggested using the GPS global navigation satellite system. This technique that provides information on total electron content (TEC) along a radio path satellite—ground receiver is sensitive enough to detect the ionospheric response to transient and periodic disturbances in the ULF band (Watson et al. 2015; Belakhovsky et al. 2016). The case study of a TEC response to an IP shock by Jin et al. (2016) suggested that a shock-generated TEC variation is a "duplication" of the shock aurora observed by UV sensors onboard the Defense Meteorological Satellite Program (DMSP) satellites. However, the idea that TEC variation is merely a "duplication" of the shock aurora met with some issues. The observed shock-generated TEC enhancement was a single 2–3-min pulse with a delayed start and peak time indicating the propagating shock compression, while the diffuse shock aurora can last much longer, ~10–20 min. Therefore, a possible mechanism for the modification of the ionosphere by a magnetospheric ULF disturbance has not been firmly established. An examination of the impact on the ionosphere by disturbances of different physical natures with simultaneous data from magnetometers, riometers, ionospheric radars, and GPS/TEC receivers may provide an insight into the mechanism of the magnetosphere–ionosphere coupling.

The IP shock impact has an important practical aspect as a driver of geomagnetically induced currents (GICs). GICs represent a significant challenge for society, given its strong dependence on a stable electricity supply (e.g., Knipp 2015 and references therein). GICs arise from induced geoelectric fields that are caused by geomagnetic field variations. The largest GICs are produced by fast changes in the geomagnetic field (dB/dt). The main phase of a geomagnetic storm or onset of a substorm is a cause of a high dB/dt and, therefore, is a risk factor for power systems at high latitudes. For example, the Hydro Quebec collapse was associated with a storm-related $dB/dt = $ ~480 nT/min. However, GIC impacts to power systems have been observed at much smaller rates of $dB/$

Belakhovsky *et al. Earth, Planets and Space* (2017) 69:105

Page 3 of 25

dt = ~100 nT/min (Kappenman 2006). Some power system failures have been associated with the occurrence of a SC or sudden impulse (SI) prior to the storm main phase (Zhang et al. 2015). Although the ΔB associated with SC/SIs is small compared to ΔB during substorms, the dB/dt can still be large enough to induce dangerous GICs in power systems. As an example, the destruction of the New Zealand power system transformer reported by Béland and Small (2004) coincided with a SC. Disturbances with dB/dt > 100 nT/min can occur during SC in the auroral region, and the magnitude of the SC-associated dB/dt is not necessarily related to the intensity of the following magnetic storm (Fiori et al. 2014).

In this study, we consider the magnetospheric and ionospheric response to the IP shock on January 24, 2012, as observed with satellite magnetometers and particle detectors, ground magnetometers and riometers, aurora imagers, and the EISCAT radar. In addition, we have used data from the GPS satellite navigation system to reveal an ionospheric response to the IP shock. We attempt to compose a comprehensive pattern of the global magnetosphere–ionosphere response, because such multi-instrument studies can provide modelers with the potential to cross-calibrate different effects. In our case study, we attempted to consider some fine details of the geomagnetic field, ionosphere, and auroral response to IP shocks using local multi-instrument observations. In particular, we examined the correspondence between the fine structure of the SC geomagnetic disturbance with the auroral, ionospheric, and TEC short-time variations. We discuss the features of the SC-related phenomena that are well understood and those that still require further consideration and modeling.

Interplanetary shock on January 24, 2012

The arrival of an IP shock is revealed according to the OMNI database on January 24, 2012, at ~1500 UT as a rapid jump in the solar wind velocity from ~400 up to ~700 km/s, an interplanetary magnetic field (IMF) magnitude B increase from ~3 up to ~30 nT, and the enhancement of the solar wind density N up to ~15 cm^{-3}. The shock impact occurs during northward IMF B_z = ~15 nT. The resultant increase in the solar wind flow dynamic pressure is P = ~10 nPa. However, the OMNI database shows a pre-shock spike (a few minutes before the arrival of the IP shock). The examination of the WIND satellite raw magnetic and plasma 3-s data reveals that this pre-shock spike is the result of an error introduced by the algorithm in the OMNI database, predicting propagated solar wind data to the subsolar bow shock.

Therefore, we present the 1-min solar wind and IMF data from the GEOTAIL satellite, located at a point with GSE coordinates (30.25, −0.62, 3.15) R_E during the encounter with the IP shock. The IP shock arrives at GEOTAIL on ~1500 UT, when the solar wind and IMF parameters increased to N = ~20 cm^{-3}, B = ~20 nT, and B_z = ~15 nT (Fig. 1). The observed step-like jumps in the plasma density, velocity, temperature, and IMF magnitude evident in Fig. 1 make it possible to associate the recorded parameters from the GEOTAIL disturbance with a fast forward shock.

This shock causes an increase in SYM-H index to ~20 nT and a short impulsive increase in the auroral electrojet index (AE) to ~800 nT (Fig. 1). After that, the AE remained at elevated levels.

Geomagnetic response on the ground to SC

We analyze data from latitudinal networks of magnetic stations in different local time (LT) sectors. The codes of the selected stations, their geographic coordinates, and geomagnetic latitudes Φ and longitudes Λ are given in Table 1. The locations of magnetic stations, riometers, optical images, and GPS receivers are shown in Fig. 2. Movements of the pierce points of the satellite/GPS receiver radio paths intersecting the ionosphere at 300 km are shown for the period 1500–1530 UT.

During the SC, the noon meridian is near the eastern coast of Canada, and the CARISMA magnetometer array (Mann et al. 2008) is in the morning sector. The profile of the CARISMA stations along geomagnetic longitude Λ of ~330° showing SC-associated magnetic disturbances at various latitudes in the morning sector (LT = ~8.5) is shown in Fig. 3. A negative PI (marked by the empty triangle) preceding a positive MI is observed at very high geomagnetic latitudes only, Φ > 72°. At lower latitudes (below ~68°), only positive MI (marked by the filled triangle) is recorded.

In this LT sector, the MI triggers quasi-monochromatic slowly decaying pulsations (coined Psc4–5 by Saito and Matsushita (1967)) at various latitudes, with periods from T = ~5 min at $\Phi \sim 72°$ (RANK) to T = ~1.5 min at Φ = ~58°–60° (PINA and THRF). An oscillatory response at intermediate latitudes Φ = ~66° (GILL) is lacking.

The stations along the Russian Arctic shore (AMD, DIK, TIX, and PBK) are in the night sector. The signature of the SC-associated PI and MI can be seen even at some of those nighttime stations (e.g., TIX). The SC triggers the development of a magnetic bay at PBK with amplitude up to ~500 nT (Fig. 4), though the IMF B_z remains northward both before and after the IP shock. The auroral indices demonstrate a bursty increase during SC up to AE = ~800 nT (Fig. 1), amplitude upper index (AU) = ~500 nT, and amplitude lower (AL) = ~−300 nT (the latter are not shown). The SC triggers a "compression" bay at PBK, while a further association of this magnetic bay with a substorm needs more evidence.
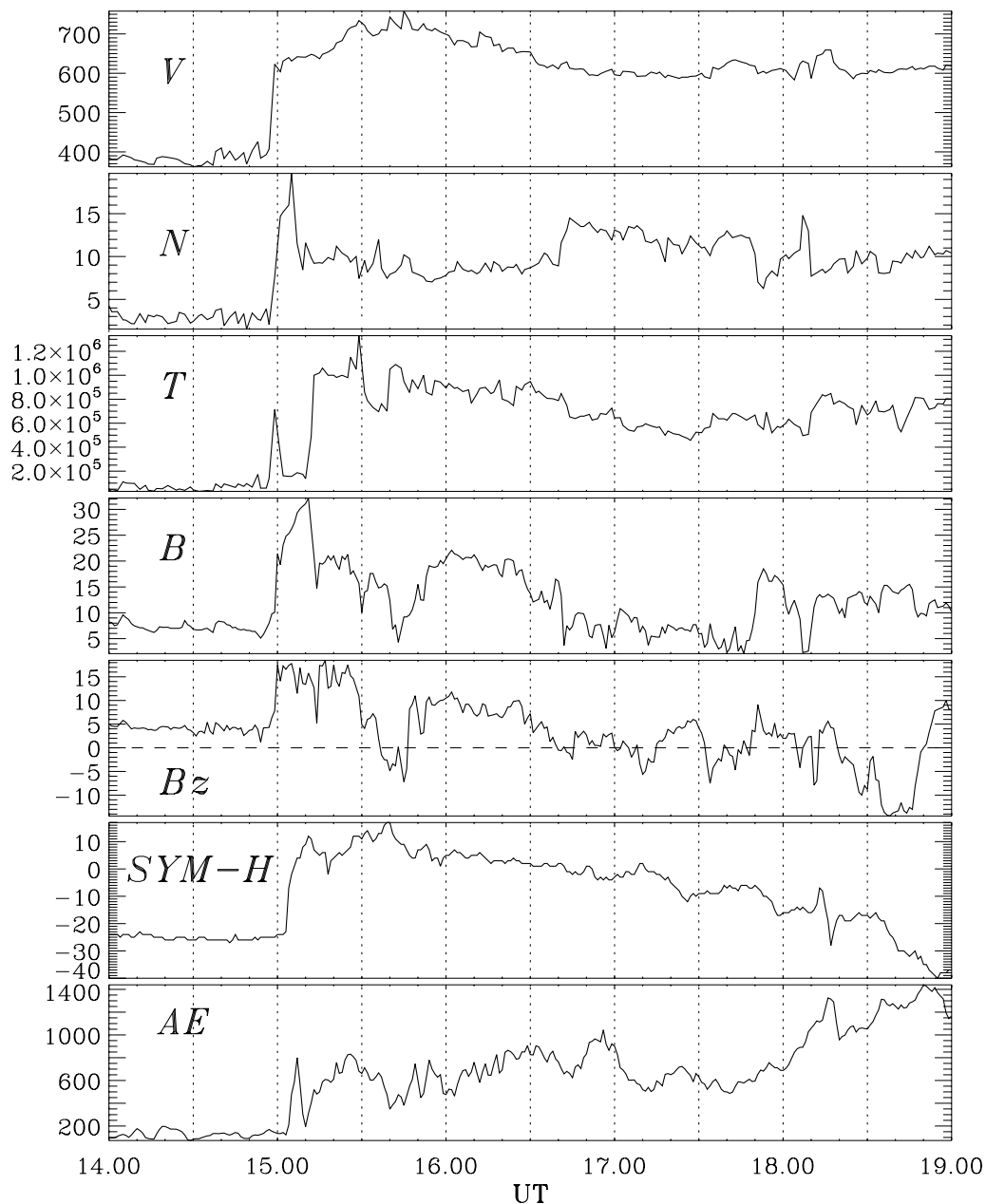
Belakhovsky *et al. Earth, Planets and Space* (2017) 69:105

Page 4 of 25

Fig. 1 The interplanetary shock detected on January 24, 2012, during time interval 1400–1900 UT by GEOTAIL: the solar wind velocity [V_x component (km/s)], solar wind density N (cm^{-3}), plasma temperature (K), IMF magnetic field magnitude B (nT) and component B_z (nT), SYM-H index (nT), and AE index (nT)

We analyze in detail the multi-instrument data from the dusk sector LT = ~17 (Scandinavia) (Fig. 2). The IMAGE magnetometers (Tanskanen 2009) record a "classical" SC, with a positive MI and a preceding negative PI at 1504 UT (Fig. 5). At a latitude of ~67°, the PI changes its polarity from negative (TRO) to positive (NOR), while the MI changes polarity between 68° and 74°. This polarity reversal of the geomagnetic disturbance is commonly

interpreted as evidence of a vortex-like structure of the ionospheric currents associated with PI and MI.

At latitudes of ~65°–67° (NOR, IVA, TRO, and SOD), fast-decaying transient Psc5 pulsations with T = ~5–6 min are triggered by the SC (Fig. 5). A period of these pulsations is latitude dependent, so they can be associated with Alfvenic oscillations of different geomagnetic shells, but not with cavity oscillations. Their

Belakhovsky *et al. Earth, Planets and Space* (2017) 69:105

Page 5 of 25

Table 1 Magnetometers, riometers, and GPS receivers

Stations	Code	Geographic latitude (°)	Geographic longitude (°)	Geomagnetic latitude (°)	Geomagnetic longitude (°)
Ny Alesund	NAL	78.92	11.95	75.2	112.1
Longyearbyen	LYR	78.20	15.82	75.1	113.0
Barentsburg	BAR	78.07	14.23	75.4	110.4
Hornsund	HOR	77.00	15.60	74.1	109.6
Hopen Island	HOP	76.51	25.10	73.1	115.1
Bear Island	BJN	74.50	19.20	71.5	108.1
Nordkapp	NOR	71.09	25.79	67.7	109.4
Tromso	TRO	69.70	18.94	66.6	102.9
Abisko	ABK	68.35	18.82	65.3	101.8
Ivalo	IVA	68.56	27.30	65.1	108.6
Kiruna	KIR	67.84	20.42	64.7	102.6
Sodankyla	SOD	67.37	26.63	63.9	107.3
Oulu	OUJ	64.52	27.23	60.9	106.1
Hankasalmi	HAN	62.25	26.60	58.7	104.5
Jyväskylä	JYV	62.42	25.28	58.5	105.7
Lovozero	LOZ	67.97	35.08	64.2	114.5
Dixon	DIK	73.50	80.60	67.9	155.7
Tixie	TIX	71.59	128.78	65.7	196.9
Pebek	PBK	70.83	170.90	64.8	223.3
Amderma	AMD	69.47	61.42	61.7	147.7
Taloyoak	TALO	69.54	266.45	72.3	330.9
Rankin Inlet	RANK	62.82	267.89	72.2	336.0
Fort Churchill	FCHU	58.76	265.92	68.3	333.5
Gillam	GILL	56.37	265.36	66.0	333.1
Sanikiluaq	SNKQ	56.50	280.80	66.5	357.0
Island Lake	ISLL	53.86	265.34	63.6	333.4
Pinawa	PINA	50.20	263.96	60.0	331.7
Thief River Falls	THRF	48.03	263.64	57.8	331.5

waveforms differ considerably from the Psc4–5 pulsations on the morning flank (Fig. 3). Therefore, the oscillatory responses of the magnetosphere on the IP shock at the morning and evening flanks are independent.

A detailed examination of the PI at stations IVA–SOD–OUL–HAN, covering latitudes from ~59° to ~65° (Fig. 5), reveals its apparent poleward propagation. This effect may be interpreted as a delay owing to different Alfven pulse propagation times from an excitation region in the equatorial magnetosphere toward the ionosphere along different field lines with latitude-dependent Alfven periods $T_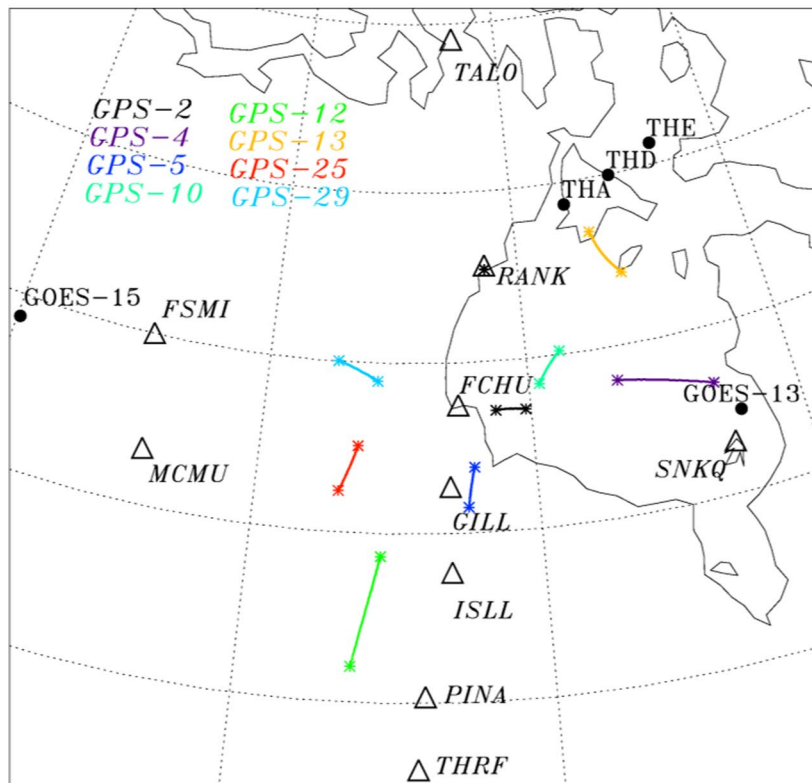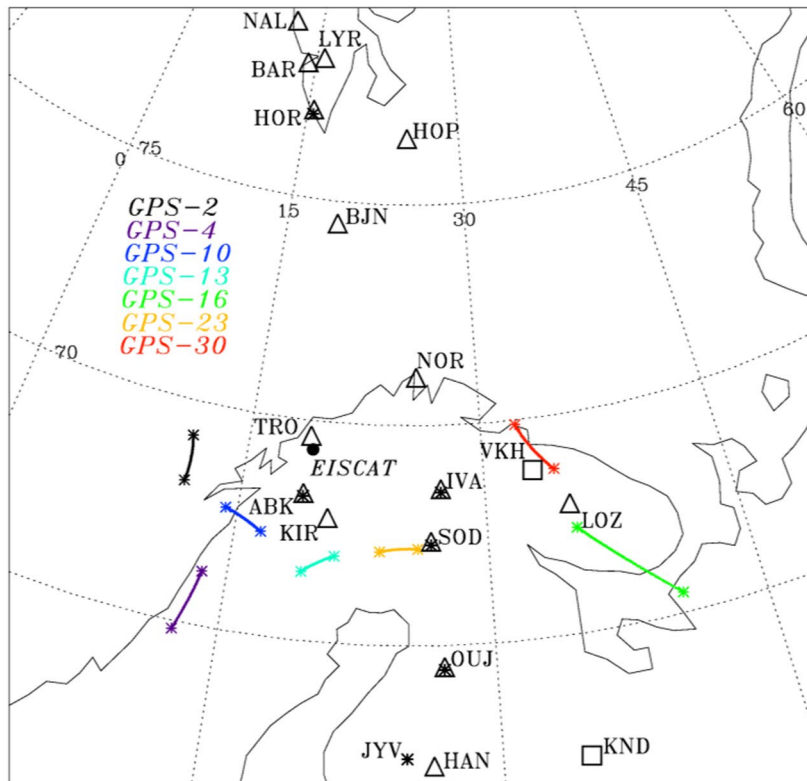A(\Phi)$. A peak of the MI also demonstrates poleward propagation, but with an apparent velocity even larger than that of the PI.
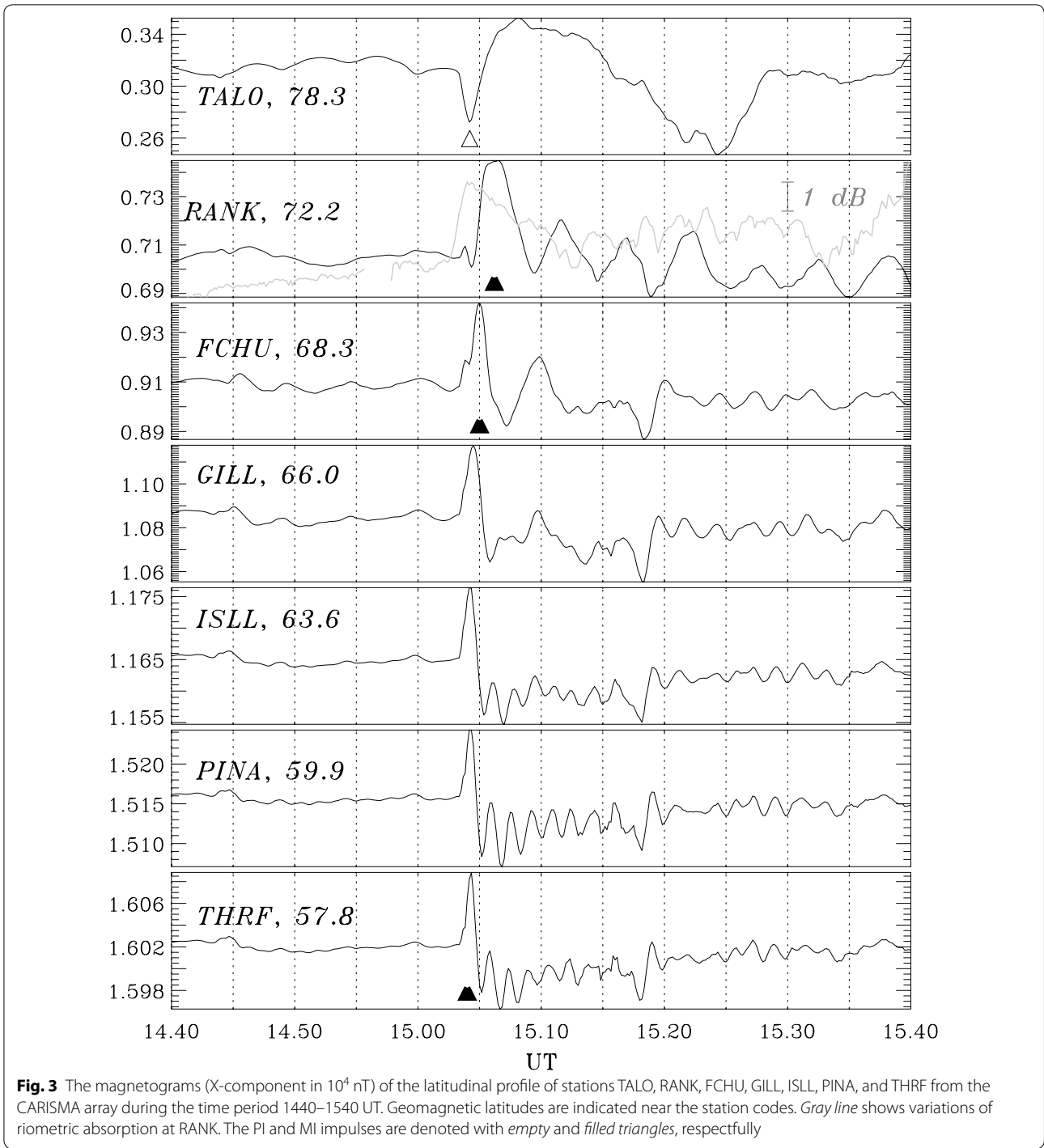
Magnetic and particle response to SC in the near-Earth space

During this event, the THEMIS-A, D, and E probes are near the morning side magnetopause (in GSE coordinates $X = \sim 5\ R_E$, $Y = \sim -8\ R_E$) above the magnetospheric equatorial plane ($Z \sim 5\ R_E$). With respect to the distance from the Earth, they are located at 1503 UT in the following order: probe E ($11.43\ R_E$), D ($11.37\ R_E$), and A ($11.21\ R_E$). Their geomagnetic projections are shown in Fig. 2

(See figure on next page.)
Fig. 2 A map with selected magnetometers (*triangles*), riometers (*asterisks*), and GIC stations (*boxes*) in Scandinavia used for the study of the SC event on January 24, 2012 (*upper panel*). Movement of the GPS pierce points (intersections with the ionosphere at 300 km of raypaths between GPS satellite and ground receiver) during the period 1500–1530 UT is shown by *a line between two asterisks*. *Bottom panel* the same as in the *upper panel*, but for Canada. *Dark dots* denote the geomagnetic projections of the THEMIS and GOES satellites
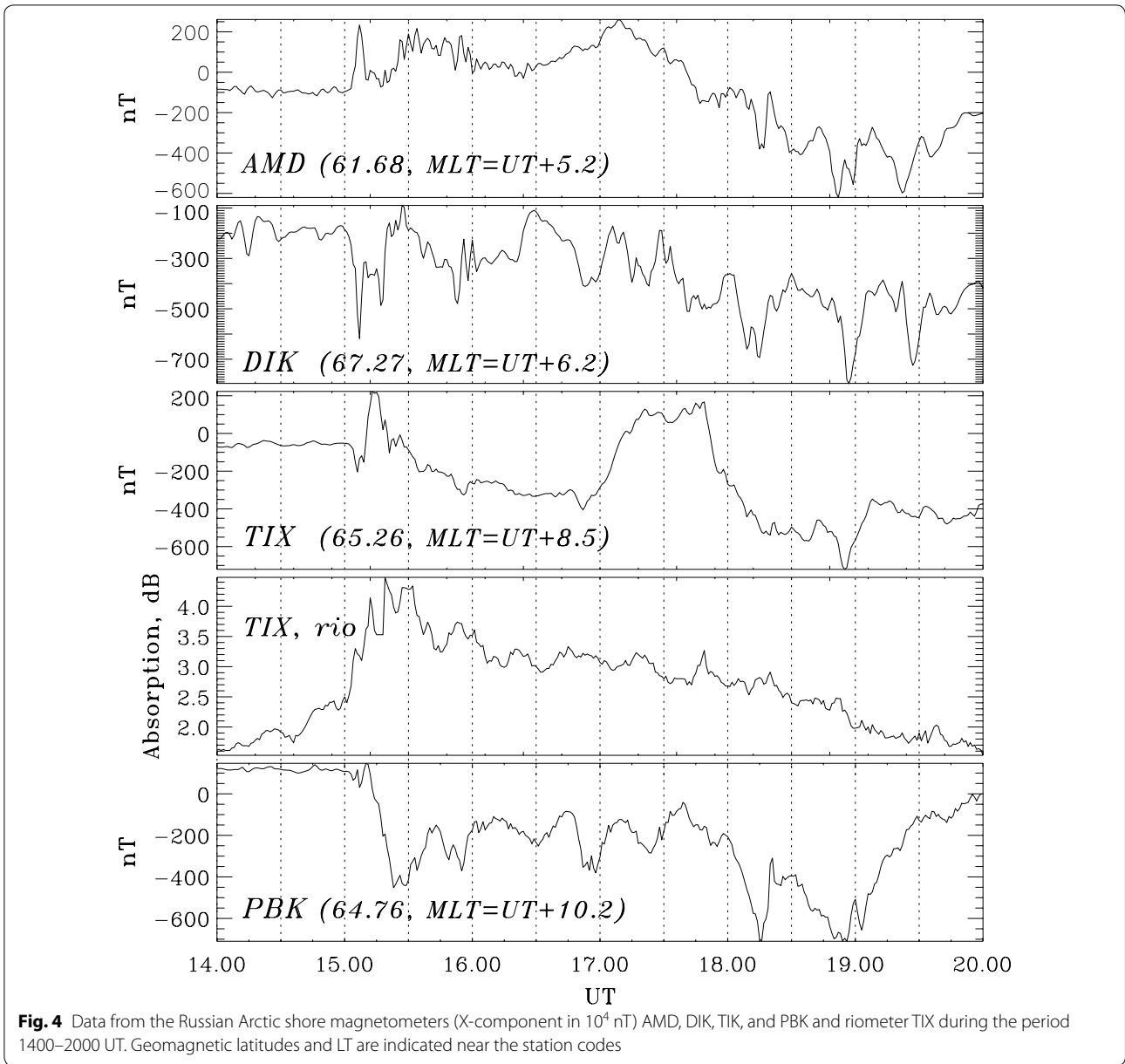
Belakhovsky *et al. Earth, Planets and Space* (2017) 69:105

Page 6 of 25

Belakhovsky *et al. Earth, Planets and Space* (2017) 69:105

Page 7 of 25

Fig. 3 The magnetograms (X-component in 10^4 nT) of the latitudinal profile of stations TALO, RANK, FCHU, GILL, ISLL, PINA, and THRF from the CARISMA array during the time period 1440–1540 UT. Geomagnetic latitudes are indicated near the station codes. *Gray line* shows variations of riometric absorption at RANK. The PI and MI impulses are denoted with *empty* and *filled triangles*, respectfully

(bottom panel). The satellite data are presented in the solar magnetospheric (GSM) coordinate system, with the X-axis directed toward the Sun, the XZ plane containing the dipole axis, and Y toward the dusk.

The THEMIS onboard magnetometers detect a strong compression of the magnetospheric magnetic field at ~1503:15 UT with an amplitude $\Delta B = $ ~70–80 nT (Fig. 6, upper panel). About 30 s later, a short pulse of the plasma Earthward (anti-sunward) speed is detected with a peak amplitude V_x ~ 1000 km/s (probe E), ~700 km/s (probe D), and ~300 km/s (probe A). The plasma density N_p starts to grow gradually ~40 s later.

Belakhovsky *et al. Earth, Planets and Space* (2017) 69:105

Page 8 of 25

Fig. 4 Data from the Russian Arctic shore magnetometers (X-component in 10^4 nT) AMD, DIK, TIK, and PBK and riometer TIX during the period 1400–2000 UT. Geomagnetic latitudes and LT are indicated near the station codes

Detailed comparison of the compressional front recorded by the THEMIS probes reveals a clear propagation effect, indicating the time delay between the compression fronts in component B_t at probes E and D of $\Delta t = 15$ s and between probes D and A of $\Delta t = 10$ s (Fig. 6, top panel). These delays correspond to the apparent velocity of the magnetic compression propagation $V_{ED} = \sim 300$ km/s and $V_{DA} = \sim 240$ km/s. For the simultaneously recorded local plasma and magnetic field parameters ($N_p = 0.8$ cm^{-3}, background electron temperature $T_e = 800$ eV, and $B = 75$ nT), the local Alfven velocity is V_A (km/s) $= 22 B$ (nT)$/\sqrt{N}$ (cm^{-3}) $= \sim 1800$ km/s, and

the sound velocity is $V_s = \sim 280$ km/s. The estimated compression front propagation velocity, neglecting the wave front orientation, is much less than the local Alfven velocity, so the Alfven Mach number is estimated to be $M_A = \sim 0.2$.

There is the possibility of estimating the shock velocity V_{sh} and shock normal to the front n from single point measurements using the coplanarity theorem (i.e., the absence of E parallel to n) from the relationships (Oliveira 2017):

$$V_{sh} = \frac{\rho_2 \vec{v}_2 - \rho_1 \vec{v}_1}{\rho_2 - \rho_1} \vec{n} \quad \vec{n} = \pm \frac{(\vec{B}_1 - \vec{B}_2) \times (\vec{B}_1 \times \vec{B}_2)}{\left| (\vec{B}_1 - \vec{B}_2) \times (\vec{B}_1 \times \vec{B}_2) \right|},$$

Belakhovsky *et al. Earth, Planets and Space* (2017) 69:105
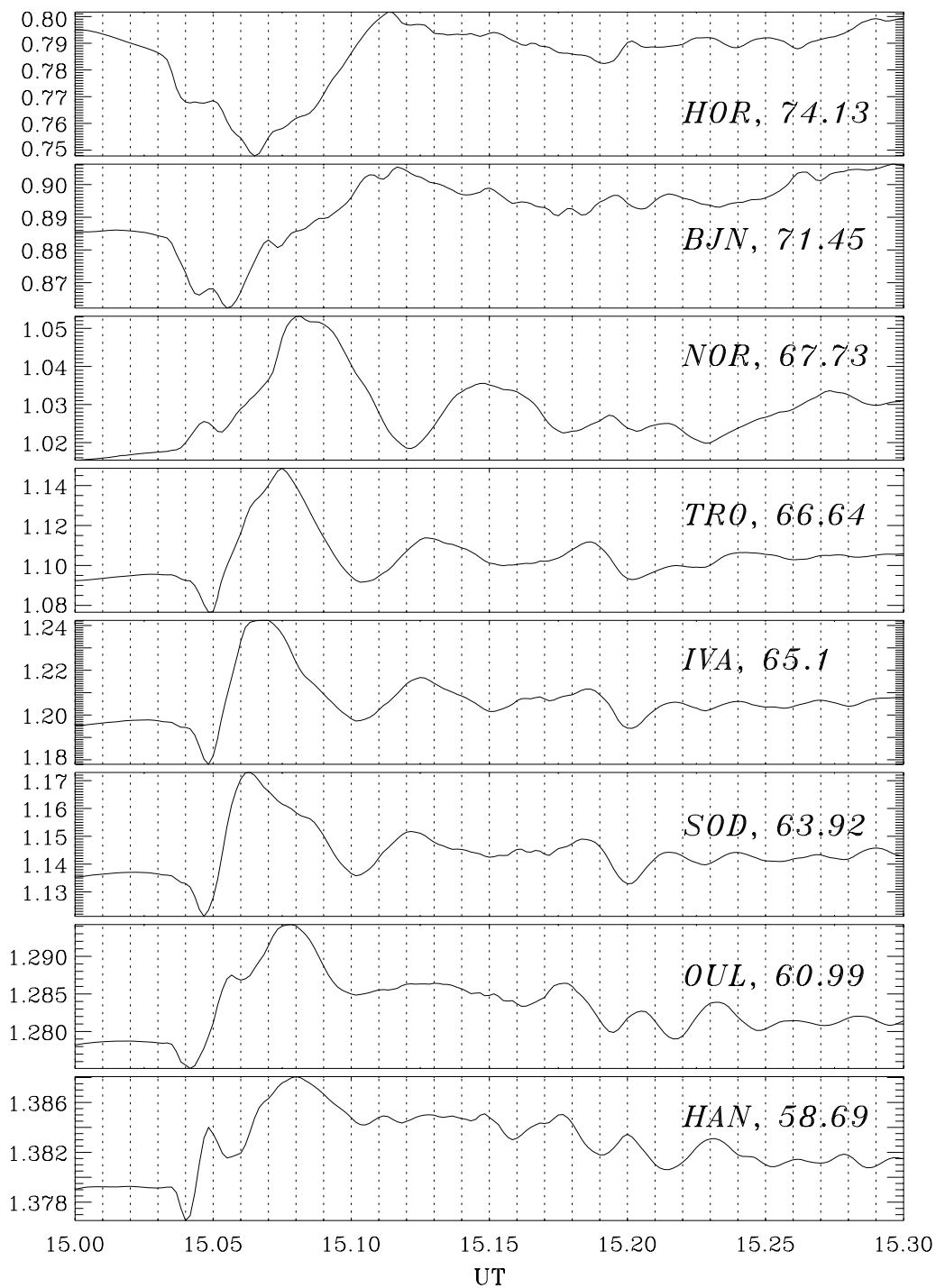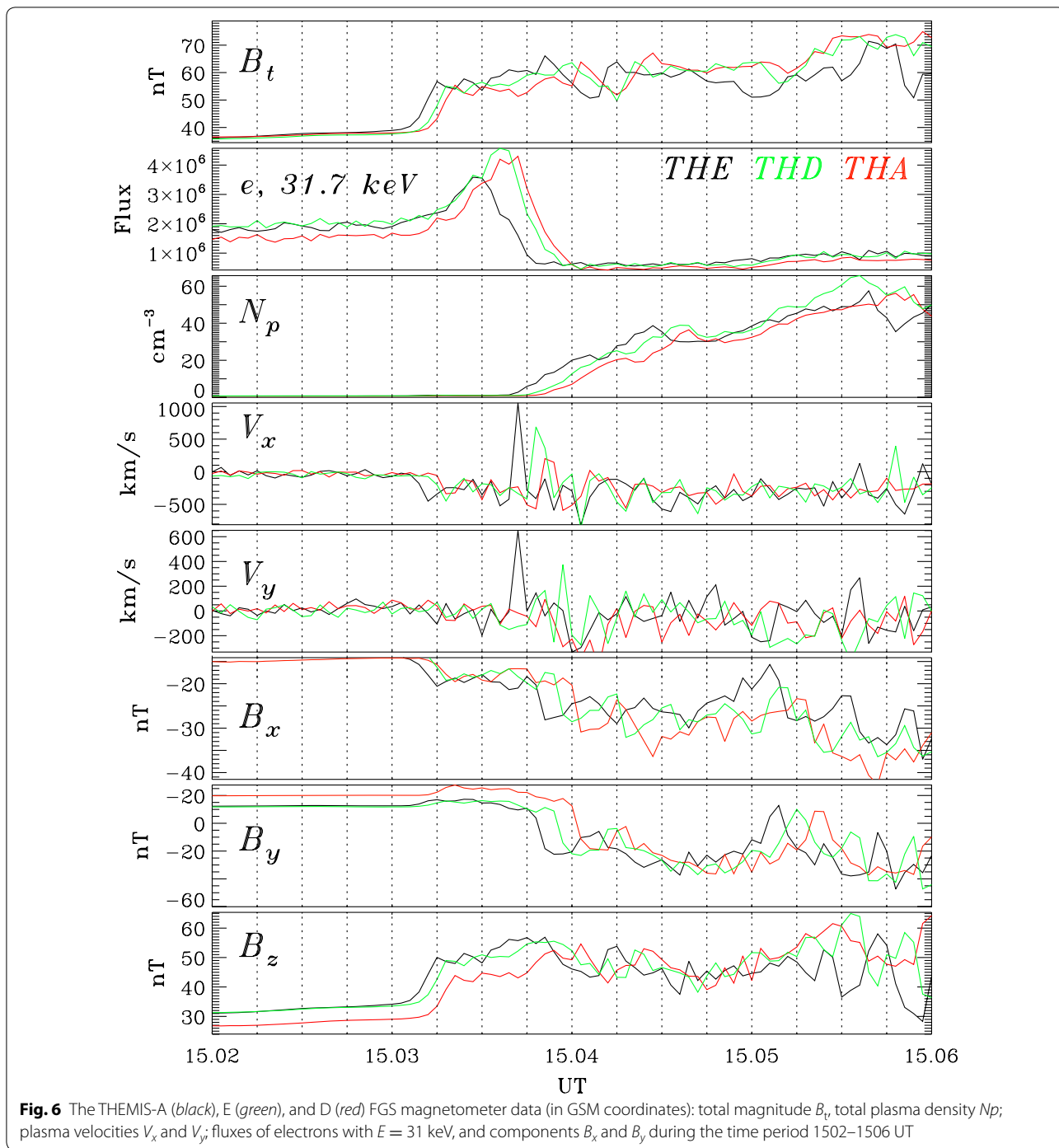
Page 9 of 25

Fig. 5 The magnetometer data (X-component in 10^4 nT) along the latitudinal profile HOR-BJN-NOR-TRO-IVA-SOD-OUL-HAN from the IMAGE array during the time period 1500–1530 UT

where ρ and V are the plasma density and velocity and B is the magnetic field vector. The indices 1 and 2 denote the medium parameter prior to (upstream) and after (downstream) a shock, respectively.

According to the Harvard-Smithsonian Center for Astrophysics IP shock database (www.cfa.harvard.edu/shocks/wi_data), the shock under study is a fast forward shock with the front normal orientation characterized by

Belakhovsky *et al. Earth, Planets and Space* (2017) 69:105

Page 10 of 25

Fig. 6 The THEMIS-A (*black*), E (*green*), and D (*red*) FGS magnetometer data (in GSM coordinates): total magnitude B_t, total plasma density Np; plasma velocities V_x and V_y; fluxes of electrons with $E = 31$ keV, and components B_x and B_y during the time period 1502–1506 UT

the angle between the normal and geocentric solar ecliptic (GSE) X-axis $\theta xn = \sim{-30}°$ and $\phi = \sim{170}°$. Indeed, for the jump of the magnetic field and velocity owing to the IP shock recorded by WIND satellite on 1440 UT located in the solar wind at $(196, -39, -15)$ R_E, the above relationships give $V_{sh} = \sim{625}$ km/s for local $V_A = \sim{94}$ km/s

and $V_s = \sim{54}$ km/s. The resultant Alfven Mach number is $M_A = 5.8$.

An estimate using the above formulas for the time 1503 UT for the magnetic field pulse detected inside the magnetosphere by THEMIS-E gives $V_{sh} = \sim{770}$ km/s. The estimated velocity is higher than the velocity determined from

Belakhovsky *et al. Earth, Planets and Space* (2017) 69:105

Page 11 of 25

the time delay between THEMIS-D and A. Nonetheless, for local magnetospheric parameters, the Alfven Mach number is $M_A = {\sim}0.4$. Despite some discrepancies, the values of the effective Mach number obtained with both techniques indicate that the compression disturbance cannot be imagined as a shock inside the magnetosphere.

In an inhomogeneous system, a fast mode wave must be partially converted into an Alfven wave. For an azimuthally large-scale disturbance such as the SC, the excited toroidal Alfven mode should have a dominating radial component of the wave electric field E_x, an azimuthal component of the magnetic field B_y, and plasma velocity V_y. However, the expected Alfven wave signatures can hardly be found in the THEMIS data (Fig. 6).

The geosynchronous satellite, GOES-13, is in the morning sector (~10 LT) during the SC. The onboard magnetometer records the Earth's magnetic field components, with B_p perpendicular to the satellite's orbital plane, B_e pointing earthward parallel to the satellite-Earth center line, and B_n perpendicular to both B_p and B_e and pointing eastward. A strong compression of magnetospheric magnetic field (as evident from the compressional component B_p) with an amplitude $\Delta B = {\sim}70$ nT (Fig. 7) is detected. The azimuthal component B_n shows the excitation of the transient long-period toroidal Psc5 pulsations ($T = {\sim}5$–6 min) and long-lasting short-period Pc3–4 ($T = {\sim}40$–50 s) pulsations triggered by the SC-related disturbance of the azimuthal component $\Delta B_n = {\sim}10$ nT.

An immediate particle flux response to the SC looks different in different energy channels of the electron detectors. The magnetic field compression at ~1504 UT recorded by THEMIS and GOES is accompanied by a positive ~5–6 min duration pulse of flux of energetic electrons with $E > 10$ keV (Figs. 6, 7). At higher E, up to relativistic energies of ~2 MeV, this positive pulse is closely followed by a gradual increase in fluxes (not shown).

The growth of particle fluxes with $E = {\sim}30$–40 keV starts nearly simultaneously with the positive PI on the ground in the same morning sector (SNKQ) (Fig. 7). The flux of 40-keV electrons ΔJ_e rapidly increases from $\sim 4 \times 10^4$ e/(cm² s str) to $\sim 2 \times 10^5$ e/(cm² s str) (Fig. 7). A rapid enhancement, more than four times, of fluxes of electrons with relativistic energies, $E > 2$ MeV, is also observed (Fig. 7). The detected rates of increase, $\Delta J_e/J_e$, in energetic and relativistic electron fluxes are larger than the bound imposed by adiabatic betatron acceleration, $\sim \Delta B/B = {\sim}0.7$.
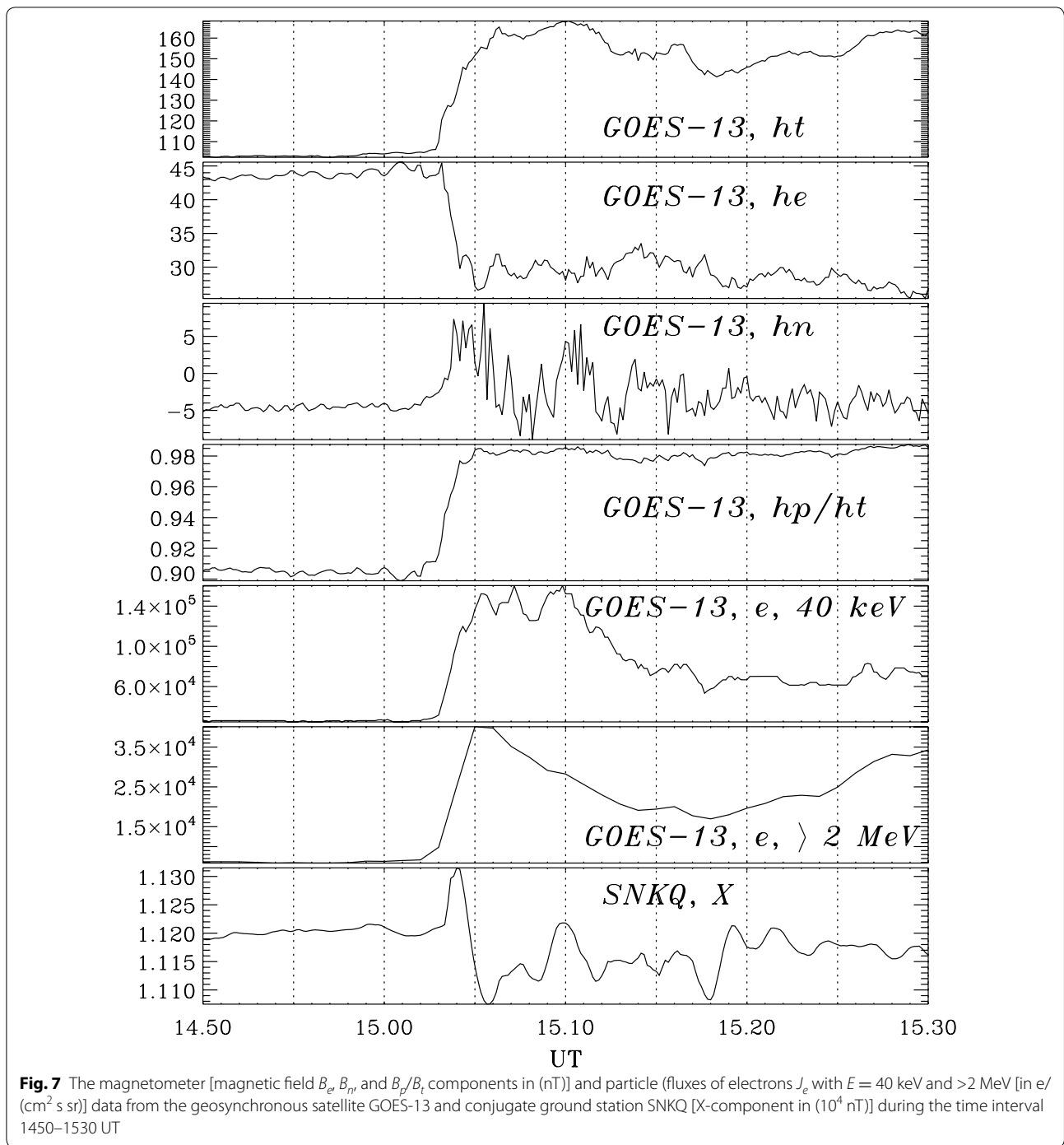
Riometer and auroral optical response to SC
Riometer observations of cosmic noise absorption provide the capability of monitoring the precipitation of

energetic electrons with $E = {\sim}30$–100 keV into the bottom ionosphere. Riometers of the Finland network show an occurrence of isolated SC-associated bursts of precipitation at all latitudes from 59° to 74° (Fig. 8). Notice a reversal of the MI polarity between ABK and HOR. The riometer data show apparent poleward propagation.

A detailed comparison of riometer absorption and geomagnetic variations (black and red lines) in the morning sector (Fig. 3) and in the post-noon sector (Fig. 8) at sites where both instruments are available demonstrates that the onset of energetic electron precipitation responsible for riometer bursts nearly coincides with the onset of PI and is slightly ahead (~1 min) of the MI. The peaks of the riometer absorption nearly coincide with the MI. In the night sector (TIX), the PI also coincides with the onset of the riometer absorption increase. The delay between the absorption onset and MI may signify either that the PI causes electron acceleration in the upper ionosphere or that the MI stimulates electron pitch angle diffusion into the loss cone in the equatorial plane. In the latter case, a time delay between the geomagnetic and riometer responses is caused by the difference of energetic (>30 keV) electron velocity and Alfven velocity upon the propagation along a field line.

The auroral response to the SC in the post-noon sector has been examined with data from two optical instruments at Svalbard. A keogram and time variations of auroral emission intensity for a fixed scan angle have been constructed from digital images from the hyperspectral all-sky camera NARUSCA II (Barentsburg) (Sigernes et al. 2012). Figure 9 shows the onset of discrete auroral forms triggered by the SC in several spectral lines. The emission lines at wavelengths 486.1 and 656.3 nm are from the proton impact excitation of hydrogen (Hβ and Hα) emissions selected for a scanning angle of −30°. The forbidden 557.7, 630.0, and 636.4 nm emissions are due to electron impact excitation of atomic oxygen [OI]. A comparison of hydrogen and oxygen emissions shows that the main proton precipitation (second panel) starts nearly simultaneously (~1509 UT) with main electron precipitation (third panel). In the SC-induced electron precipitation, the intensity of the green emission is much higher than the intensity of the red emission, in contrast to typical dayside cusp aurora. Therefore, for SC-induced precipitation, electrons with higher energies (≫1 keV) dominate.

The main growth of the auroral emission intensities is preceded by a weak intensity increase that starts around 1505 UT (Fig. 9). This auroral intensification starts nearly simultaneously with the onset of the riometer burst at NOR and the positive PI in the magnetic record at BAR.

Belakhovsky *et al. Earth, Planets and Space* (2017) 69:105

Page 12 of 25

Fig. 7 The magnetometer [magnetic field B_e, B_n, and B_p/B_t components in (nT)] and particle (fluxes of electrons J_e with $E = 40$ keV and >2 MeV [in e/ $(cm^2$ s sr)] data from the geosynchronous satellite GOES-13 and conjugate ground station SNKQ [X-component in (10^4 nT)] during the time interval 1450–1530 UT

The keogram constructed with data from the meridian scanning photometer at a somewhat higher latitude (LYR) shows a simultaneous activation of the red (630.0 nm) and green (557.7 nm) emissions (Fig. 10). The main increase in auroral intensity is preceded by a weak green line emission enhancement at scanning angle ~160° that started at

~1505 UT, simultaneous with the PI and the onset of the riometer burst (HOR). This weak enhancement has the form of three narrow auroral poleward moving arcs that eventually merge into a wide-latitude auroral increase.

The onset of the main increase in red and green emission intensities above LYR (scan angle 90°) is delayed

Belakhovsky *et al. Earth, Planets and Space* (2017) 69:105

Page 13 of 25
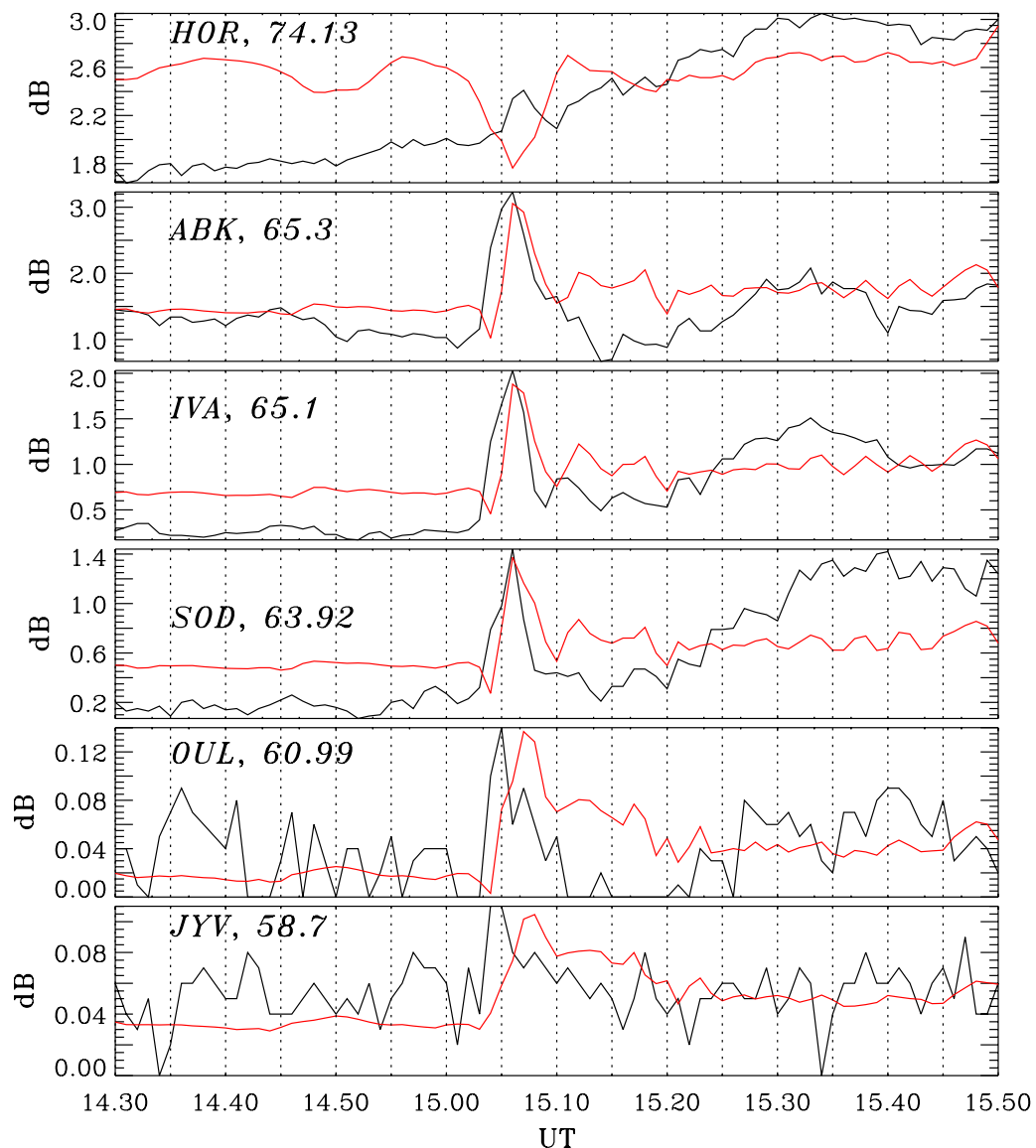
Fig. 8 Cosmic noise absorption (*black line*) and X-component magnetic field (*red line*) variation along the profile of stations HOR-ABK-IVA-SOD-OUL-JYV from the Finland riometer network and IMAGE array during 1450–1550 UT

~4 min as compared with the peak of the magnetic disturbance at LYR (Fig. 10).

Ionospheric TEC response to SC as observed by the GPS system

We have examined the TEC response using 30-s data from the worldwide GPS receivers compiled into the IGS system. The slant TEC data have been converted into vertical TEC data, vTEC.

The TEC response in the morning hours (Canadian sector) is shown in Fig. 11 (bottom panel). The location of the pierce points for all radio paths with elevation angles

$\alpha > 15°$ during the SC event is shown in Fig. 2 (bottom panel). The TEC data derived from signals from different GPS satellites received at station CHUR demonstrate that a gradual vTEC growth starts right after the SC (Fig. 11, bottom panel). The relative increase, $\Delta(vTEC)/(vTEC)$, reaches 40%. The TEC growth during the SC in the morning sector is observed at latitudes above 60° only. These variations are possibly the result of enhancement of the global electric field of the ionosphere (Nayak et al. 2016).

In the evening sector (Scandinavia), vTEC variations have been constructed for different radio paths between
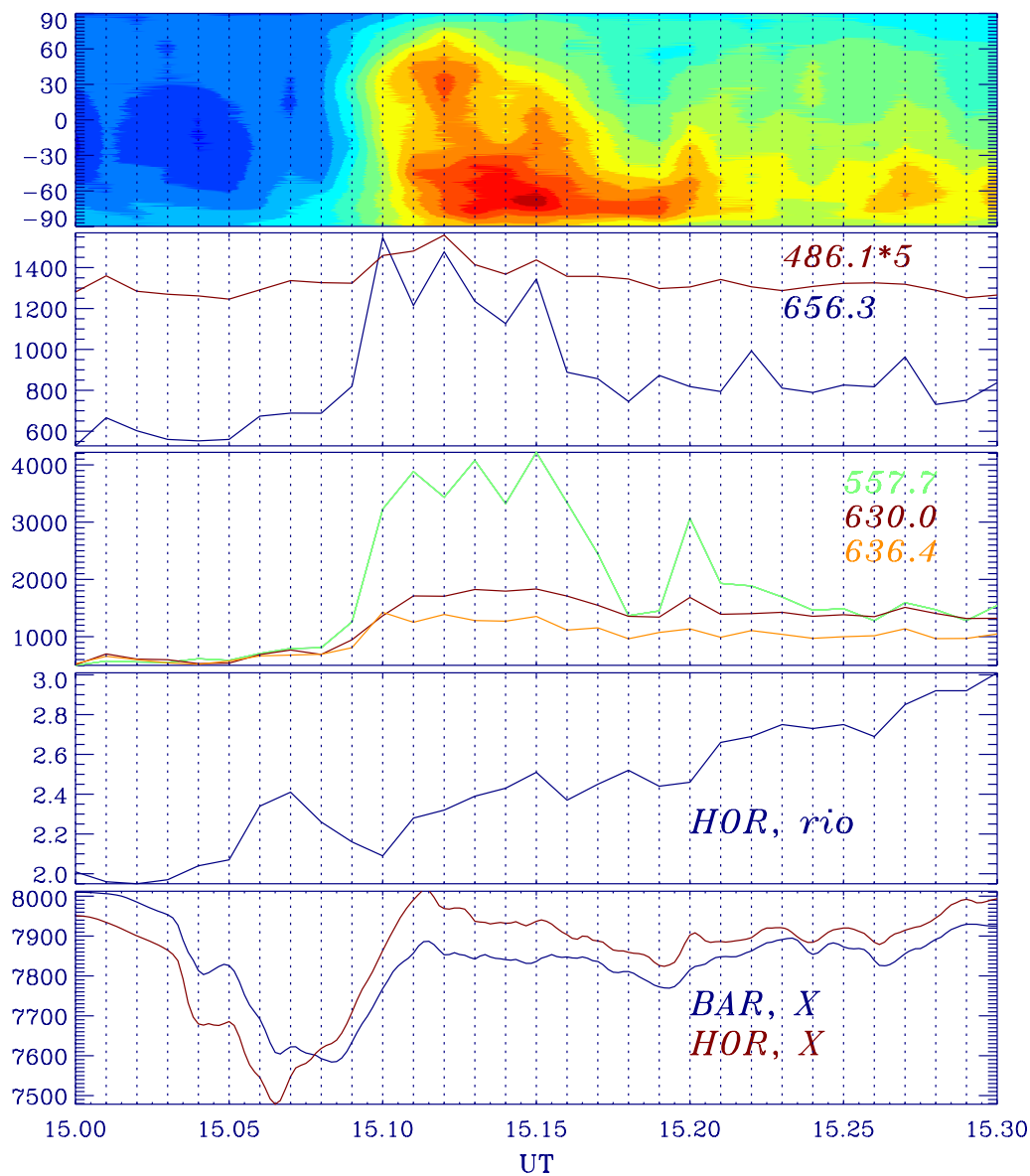
Belakhovsky *et al. Earth, Planets and Space* (2017) 69:105

Page 14 of 25

Fig. 9 Keogram of 630.0 nm emission intensity (scan angle—UT) produced from the digital image of the NORUSCA hyperspectral all-sky imager (Barentsburg); intensity variations (in Rayleigh) of emissions produced by proton precipitation 486.1 nm (multiplied by 5) and 656.3 nm, and by electron precipitation 557.7, 630.0, and 636.4 nm, riometer (in dB), and geomagnetic (X-component) (in nT) variations at stations HOR and BAR during the time interval 1500–1530 UT

available GPS satellites and the KIRU receiver. The location of relevant pierce points with $\alpha > 15°$ during the SC event is shown in Fig. 2 (upper panel). With a background of a gradual increase in vTEC, a superposed positive pulse of vTEC is observed with an amplitude up to $\Delta(vTEC) = \sim 1$ TECu (Fig. 11, upper panel). The relative increase, $\Delta(vTEC)/vTEC$, produced by the pulse is about 8–9%.

The onset of the TEC pulse coincides with the PI at station KIR, but no PI signatures can be seen in the TEC waveforms. The peak of the TEC pulse coincides with the peak of the geomagnetic MI at KIR. The observed ionospheric response may be caused by different mechanisms. To identify a responsible mechanism, it is important to determine the vertical structure of an ionospheric disturbance. Such a structure can be measured with VHF incoherent radar.
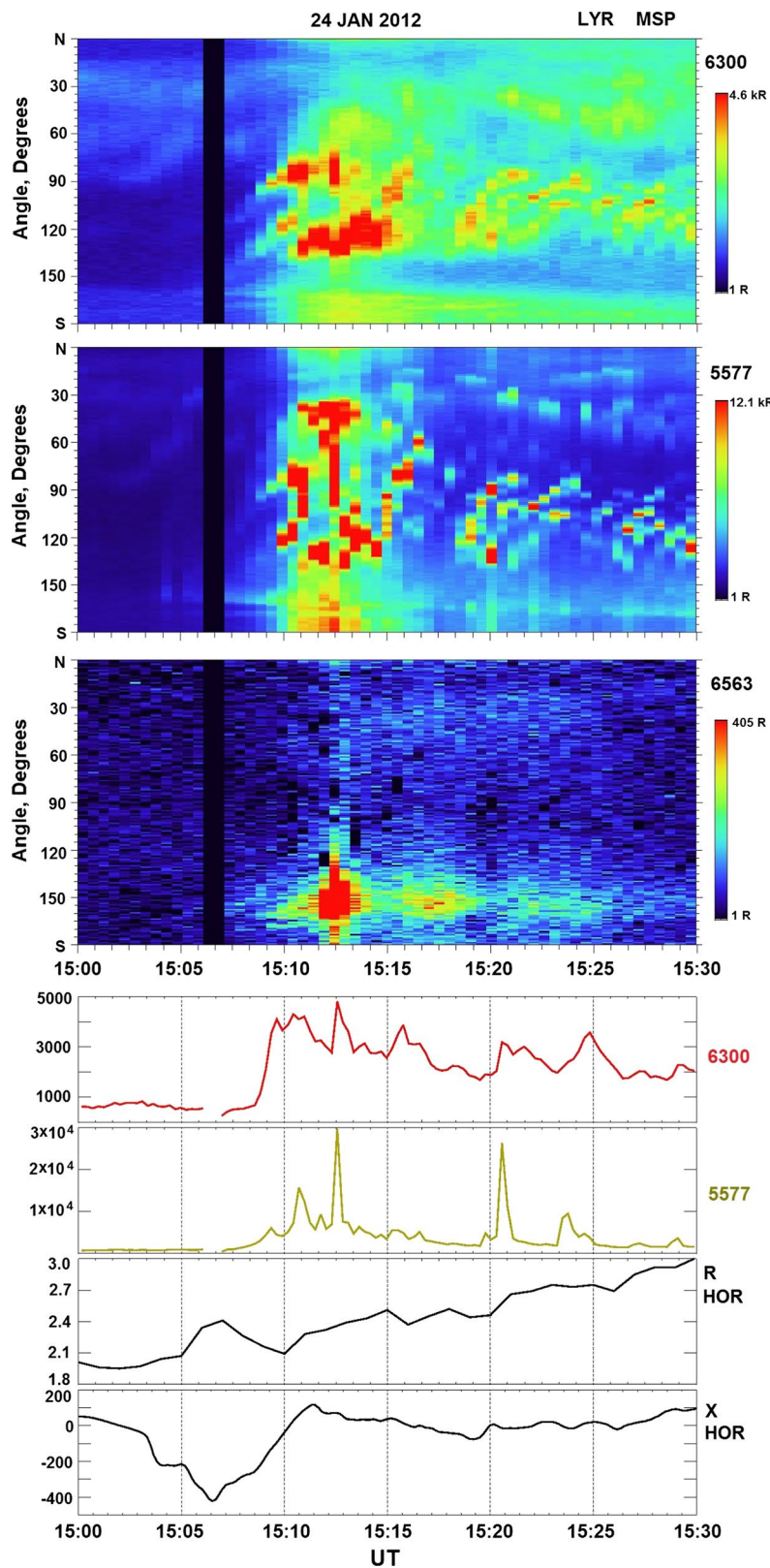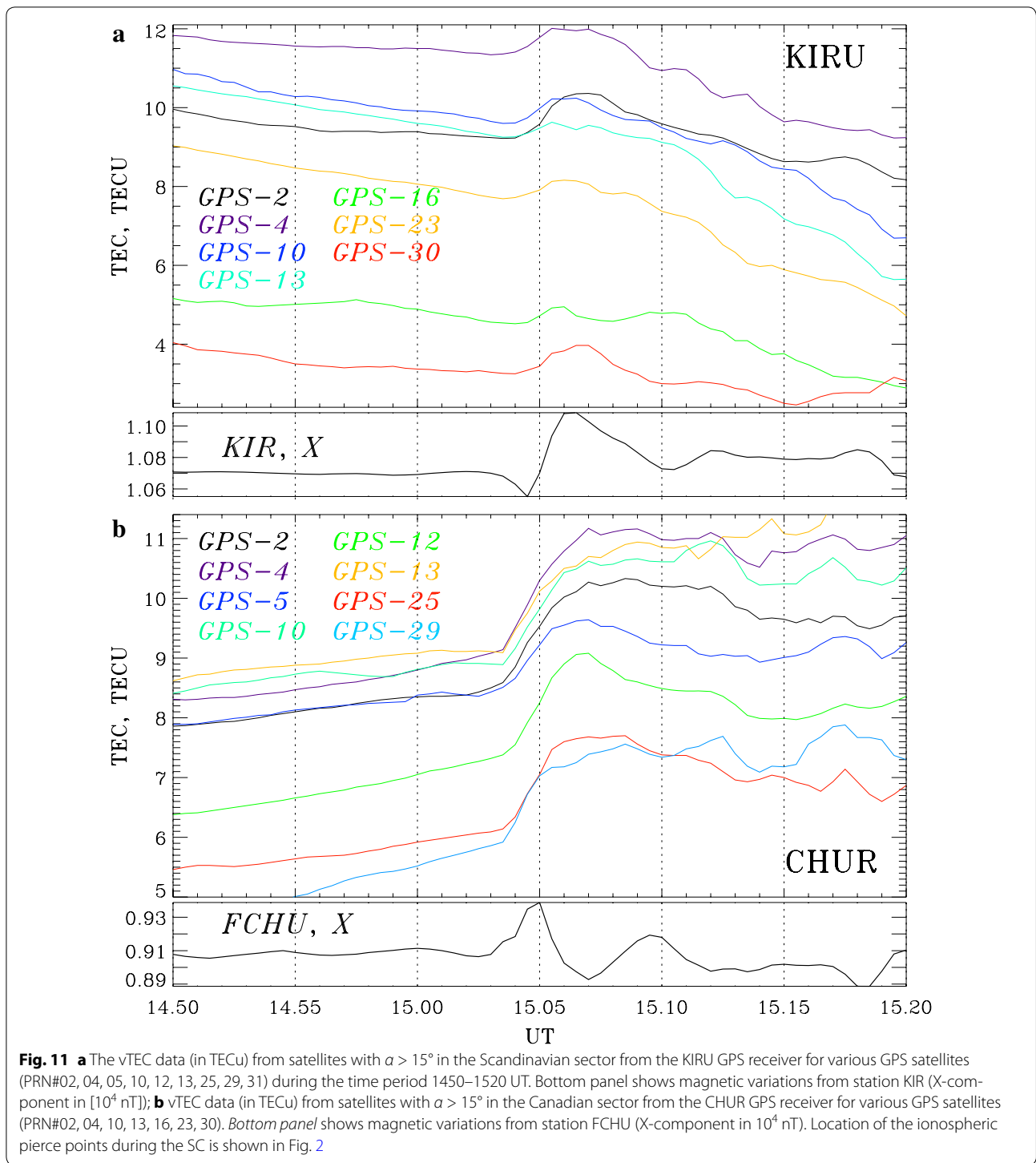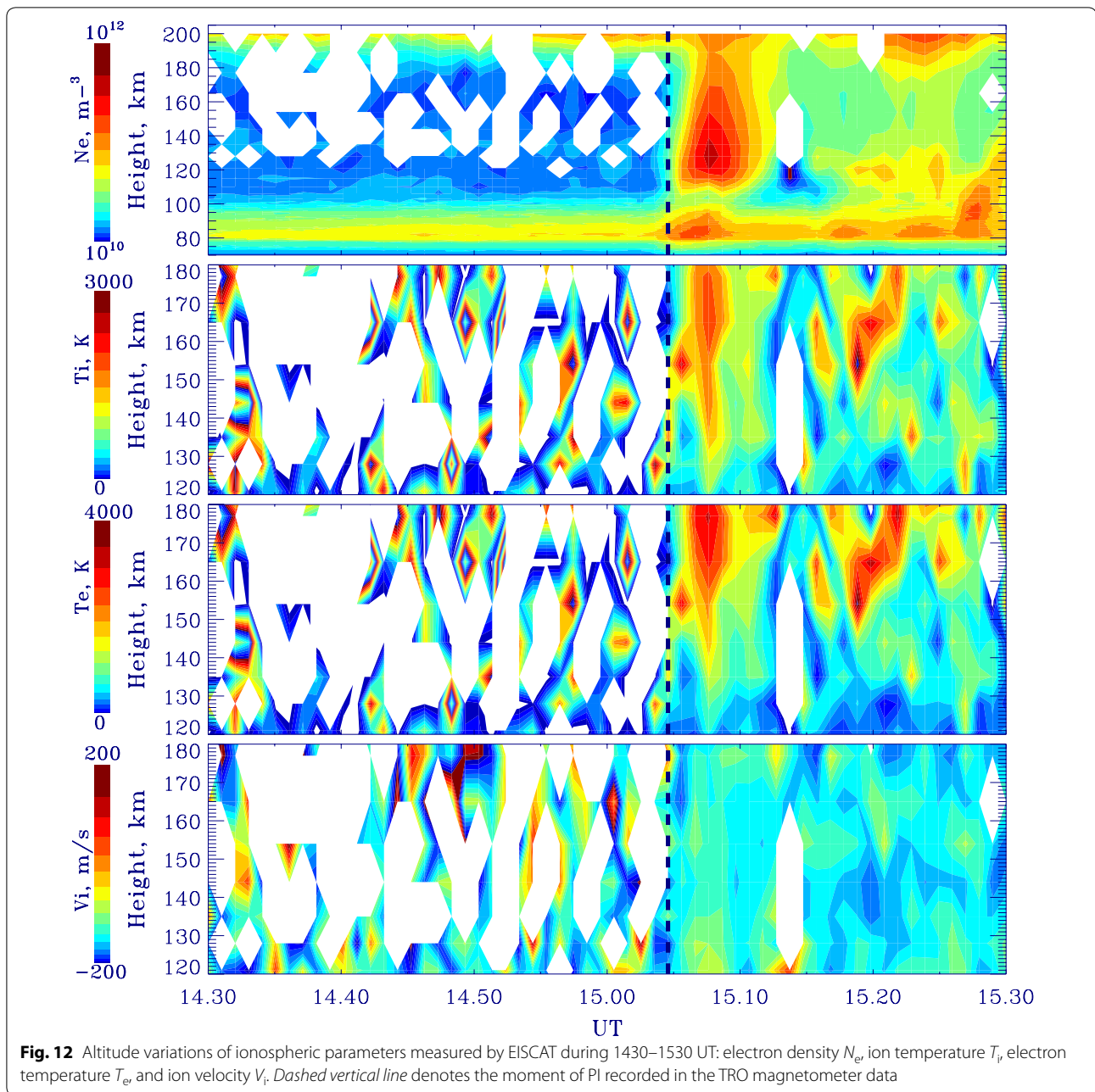
Belakhovsky *et al. Earth, Planets and Space* (2017) 69:105

Page 15 of 25

Fig. 10 Keograms of 630.0, 557.7, and 6563 nm emissions recorded by meridian scanning photometer at LYR (*upper panels*), vertical intensities of 630.0 nm and 557.7 nm emissions (in Rayleigh), riometer variations (in dB), and geomagnetic variations (X-component) (in nT) at station HOR during the time interval 1500–1530 UT

Belakhovsky *et al. Earth, Planets and Space* (2017) 69:105

Page 16 of 25

Fig. 11 **a** The vTEC data (in TECu) from satellites with *a* > 15° in the Scandinavian sector from the KIRU GPS receiver for various GPS satellites (PRN#02, 04, 05, 10, 12, 13, 25, 29, 31) during the time period 1450–1520 UT. Bottom panel shows magnetic variations from station KIR (X-component in [10⁴ nT]); **b** vTEC data (in TECu) from satellites with *a* > 15° in the Canadian sector from the CHUR GPS receiver for various GPS satellites (PRN#02, 04, 10, 13, 16, 23, 30). *Bottom panel* shows magnetic variations from station FCHU (X-component in 10⁴ nT). Location of the ionospheric pierce points during the SC is shown in Fig. 2

EISCAT radar response to the SC

The EISCAT incoherent radar system in Tromsø provides a vertical profile up to 200 km for the main ionospheric parameters with a cadence of 1 min. The EISCAT-measured electron density, N_e, evidently shows an impulsive response to the SC (Fig. 12). At the same time, no

clear signatures in the ionospheric plasma velocity V_i coherent with the magnetic disturbance are observed. EISCAT reveals sharp increases in ion and electron temperatures, T_i and T_e, at heights h > 140 km. In addition to the N_e enhancement, a short-time (1505–1509 UT) burst of electron temperature T_e at h > 150 km and ion

Belakhovsky *et al. Earth, Planets and Space* (2017) 69:105

Page 17 of 25

Fig. 12 Altitude variations of ionospheric parameters measured by EISCAT during 1430–1530 UT: electron density N_e, ion temperature T_i, electron temperature T_e, and ion velocity V_i. *Dashed vertical line* denotes the moment of PI recorded in the TRO magnetometer data

temperature T_i at $h > 140$ km is detected. The N_e burst lasts longer than the T_e and T_i bursts (from 1504 to 1511 UT).

The most evident response in the electron density N_e can be seen at $h = 100–180$ km (Fig. 13). A growth of N_e in the E-layer (120 km) starts simultaneously with the riometer increase and the PI. The increase in N_e from ~10^{10} to ~1.7×10^{11} m^{-3} reaches a maximum simultaneously with the MI peak, but decays during a period of ~2 min, which is longer than the duration of the MI

(~1 min). The onset and duration of the EISCAT-measured N_e pulse and the GPS-detected TEC pulse are nearly the same, 1504–1511 UT, which indicates that both pulses are manifestations of the same disturbance.

GIC response to the SC

An interesting and significant manifestation of the SC is the burst of GIC in the ground technological systems. The Polar Geophysical Institute (Apatity, Russia) has deployed and operated a system for recording GIC in

Belakhovsky *et al. Earth, Planets and Space* (2017) 69:105

Page 18 of 25
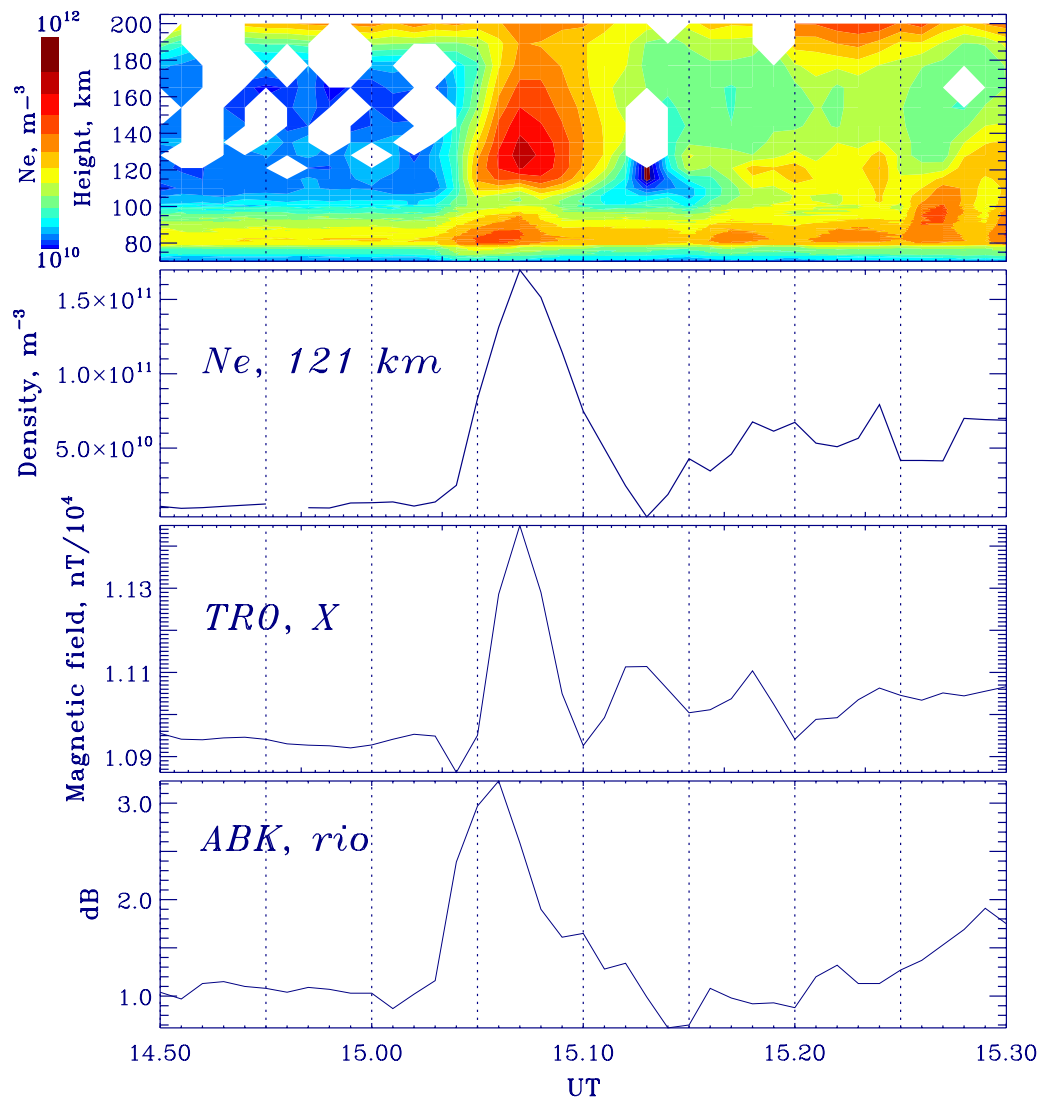
Fig. 13 Ionospheric and geomagnetic observations during January 24, 2012, at 1430–1530 UT (from *top* to *bottom*): altitude distribution of electron density N_e variations measured by EISCAT; variations of N_e at altitude $z = 121$ km; and magnetic field variations [X-component in (nT)] at TRO and riometer variations (in dB) at IVA
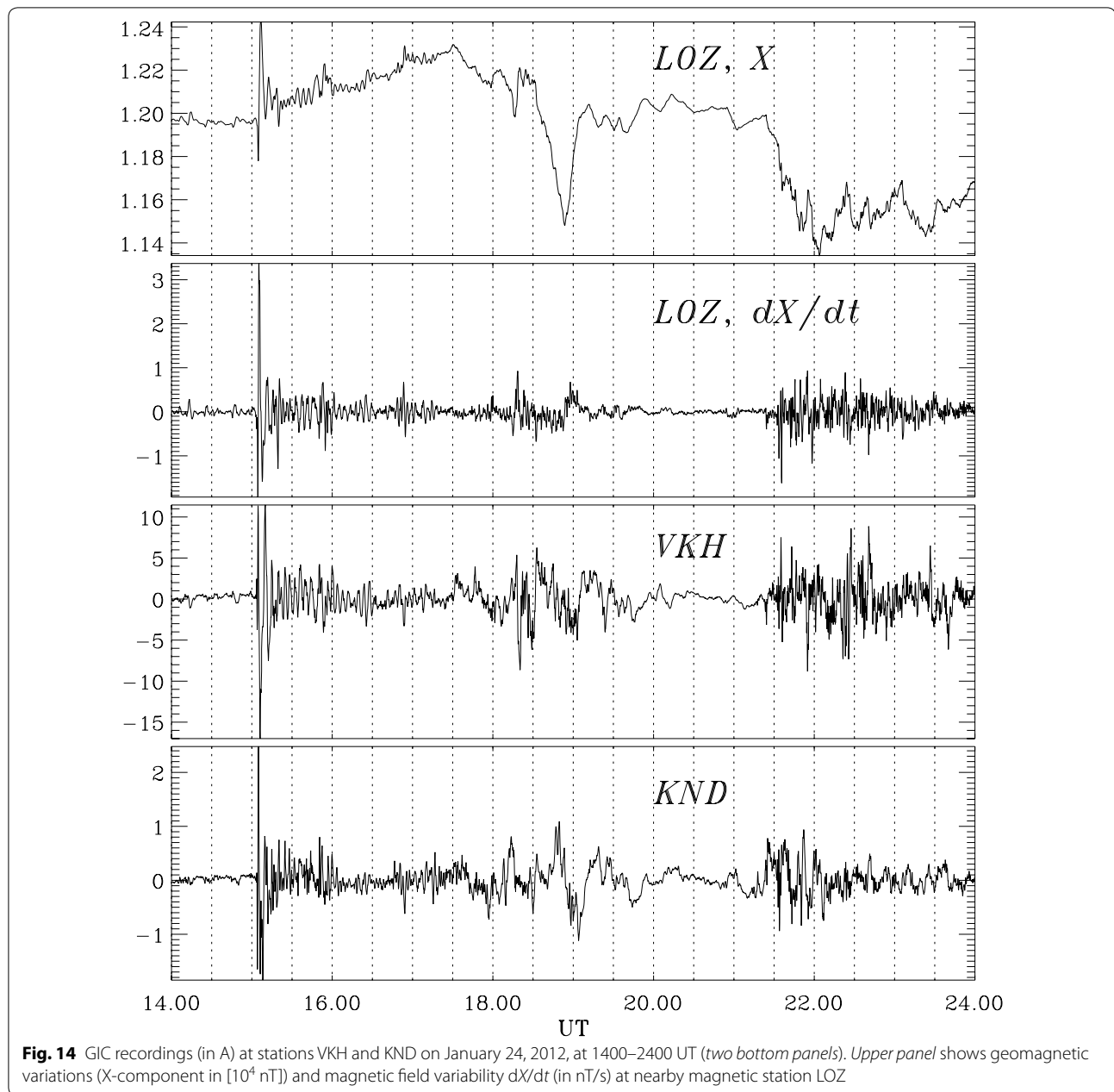
power lines since 2010 (Sakharov et al. 2009; Viljanen 2011). This system consists of five stations elongated in a latitudinal direction in the Kola Peninsula and in Karelia. In this study, we use data from the stations Vykhodnoj (VKH) with geographic coordinates 68.83°N, 33.08°E and Kondopoga (KND) with coordinates 62.21°N, 34.28°E (see map in Fig. 2, upper panel).

During the SC, a rapid burst of GIC is recorded at both stations VKH and KND (Fig. 14). The amplitude of the GIC at VKH reaches ~30 A. Variations of the GIC are similar to variations of the magnetic field derivative, dX/dt, at the nearby magnetic station LOZ. During the SC, the dX/dt level reaches ~180 nT/min. The GIC intensity

caused by the SC is about two times higher than the GIC during the subsequent substorm intensifications, though the SC amplitude (~400 nT) is less than the amplitude of the substorm-associated magnetic bay (~600 nT). This fact matches well with a higher amplitude of dX/dt during the SC as compared with that during the substorm intensifications at ~1830 UT and ~2130 UT.

Discussion: a possible mechanism of IP shock impact on the geomagnetic field and ionosphere

We have presented a comprehensive picture of the IP shock impact onto the magnetosphere, ionosphere, and geomagnetic field, as detected by various instruments.

Belakhovsky *et al. Earth, Planets and Space* (2017) 69:105

Page 19 of 25

Fig. 14 GIC recordings (in A) at stations VKH and KND on January 24, 2012, at 1400–2400 UT (*two bottom panels*). *Upper panel* shows geomagnetic variations (X-component in [10^4 nT]) and magnetic field variability d*X*/d*t* (in nT/s) at nearby magnetic station LOZ

We hope that the inter-calibration of the observed effects will help modelers to validate the models of the solar wind–magnetosphere–ionosphere coupling during the SC. Though our observations of the SC event can be basically understood in the framework of existing understanding, some features still require additional consideration and modeling.

A rapid displacement of the magnetopause caused by an IP shock induces a magnetic disturbance propagating as a fast compressional wave inward in the magnetosphere. Most of this wave energy is scattered throughout the magnetosphere, but some reaches the Earth. The ground signal is gradually built up with a time, governed by the propagation time of the MHD disturbance from different parts of the magnetopause and the time of sweeping the dayside magnetosphere by a shock. At the front of a fast compressional wave, an Alfven pulse can be generated. This pulse was suggested to produce a high-latitude PI (Nishida 1964). The transmission of an Alfven pulse through the ionosphere should cause a negative H-component disturbance at the ground, preceding a MI. Therefore, the MI and PI are two nearly overlapping wave

Belakhovsky *et al. Earth, Planets and Space* (2017) 69:105

Page 20 of 25

processes of different physical nature. However, there are still no reliable in situ confirmations of the mechanism of the PI generation at the compressional wave front. In the present event, neither the satellite magnetometers nor the plasma sensors have revealed any clear signature of excited Alfven waves. In contrast, the nature of a short pulse of earthward plasma velocity behind the magnetic compression front (at 1502:20 UT in Fig. 6) is unclear.

According to global MHD modeling (Samsonov et al. 2007), the transmitted shock should propagate as a weak shock with M_A slightly greater than 1 through the magnetosphere and then partially (~30%) reflect from the plasmapause/ionosphere. Further, the interaction of the reflected shock with the magnetopause should launch a secondary fast compressional wave moving inward into the magnetosphere, etc. This scenario in effect may suggest an effective excitation of the MHD cavity mode trapped between the magnetopause and the plasmapause/ionosphere. However, these theoretical predictions on effective reflection of a fast mode from the inner magnetosphere and subsequent formation of a cavity mode have not been supported by our observations. Upon analysis of the space and ground magnetometer data, no global coherent oscillatory response to the SC has been found. In our opinion, a very rare occurrence of the global cavity mode is a natural consequence of a weak reflection of a large-scale MHD mode with scale size ~10 R_E from a small target (Earth) with scale size ~1 R_E. The lack of cavity mode excitation in our analysis may be supported by numerical MHD simulation of IP shock impacts on the magnetosphere with different normal orientations by Oliveira and Raeder (2014). These authors concluded that the shock impact angle plays a major role in effectively compressing the magnetosphere, thereby leading to a more favorable scenario for cavity mode excitation due to symmetric magnetosphere compression. They found that inclined strong shocks did not lead to cavity wave excitation, and only shocks with normal incidence did. Since the IP shock discussed here has very similar properties to the one simulated by Oliveira and Raeder (2014), with exactly the same shock impact angle, their conclusions support the argument of the lack of cavity mode excitation in observed in the event discussed in this paper.

Only latitudinally localized transient Psc5 pulsations at the dawn and dusk flanks have been observed that correspond to the independent response of resonant field lines in the morning and evening sectors (Samsonov et al. 2011). Some characteristic features of these pulsations indicate their resonant nature, including a frequency dependence on latitude and an apparent poleward propagation along the latitudinal magnetometer array (not shown).

The lack of an oscillatory Psc5 response at intermediate latitudes, $\Phi = $ ~66°, is probably caused by the plasmapause, because in its vicinity the radial gradient of the Alfven period, $T_A(\Phi)$, becomes smooth. Therefore, a mode conversion into Alfven oscillations of a geomagnetic shell is weak in this region. Drivers with band-limited spectral content, exciting transient Alfven wave response in a limited range of latitudes only, may be different. The wave energy can be transported to a resonant magnetic shell as an evanescent large-scale magnetopause surface mode or as a waveguide/cavity mode (e.g., Hartinger et al. 2012). Both the surface mode and waveguide mode would be inevitably resonantly converted into the Alfven field line oscillations.

Our estimate of the compressional front velocity, from either timing analysis or the jump in plasma parameters, does not support the idea of the shock wave propagation pattern through the magnetosphere. All obtained values of $M_A = $ ~0.2–0.4 in the outer magnetosphere indicate that the IP shock cannot survive when propagating through the magnetosphere, so the compression front cannot be imagined as a weak shock inside the magnetosphere, in contrast to the modeling predictions (Samsonov et al. 2007). The fact that an apparent propagation velocity of the magnetic field compression is less than the local V_A does not exclude the possibility that this compression is caused by the fast mode, because in an inhomogeneous system, the group velocity of this mode is less than V_A (Allan and Wright 1998).

The equatorward portion (~65°–79°) of the morning auroral oval is occupied by energetic electron precipitation observed from the ground as a region with diffuse green emissions, while in the poleward part of the oval (~75°–83°), there is a region of soft electron precipitation corresponding to red emission aurora (Zhou et al. 2003). Diffuse green aurora is primarily caused by the precipitation of energetic electrons (0.1–30 keV) over a broad latitude range (CPS type plasma). The red discrete aurora is dominated by soft electron precipitation (0.1–1 keV), which corresponds to injections of magnetosheath plasma. Two types of responses of the dayside/morning aurora to an IP shock were observed: (1) a "fast" (in ~1 min) onset of the green diffuse aurora manifested as a relatively uniform luminosity structure in the equatorward edge of the oval and (2) a "slow" (with a delay of ~4–5 min) substantial enhancement of a discrete red emission band at a higher latitude (Motoba et al. 2009; Liu et al. 2015). This two-step development of the postnoon shock aurora supposes the operation of several mechanisms of auroral intensification. The fast response may be related to a fast magnetosonic pulse propagating across the magnetosphere from the region of the IP shock impact on the magnetopause, with a velocity ~10^3

Belakhovsky *et al. Earth, Planets and Space* (2017) 69:105

Page 21 of 25

km/s, whereas a slow intense response is caused by the disturbance propagating along the magnetospheric flanks with a shock velocity in the magnetosheath.

In the photometer observations at LYR, a response to the IP shock has been observed in the green and red channels starting at ~1505 UT in the equatorward part of the auroral oval (Fig. 10). The response develops into two polar moving arcs with comparable intensities (~1 kR) in both channels until 1509 UT, at which time the intensity of the green channel overcomes the red emission line. After this time, the green channel has three to four times the intensity of the red, and the two arcs stop their poleward movement. In addition, a new green arc is formed in the poleward part of the oval (between 30° and 60° scan angle) starting at ~1511 UT. At this time, a very strong proton arc forms, and at ~1519 UT, it completely subsides in the equatorward portion of the oval (between 130° and 165° scan angles). Therefore, our observations do not coincide completely with the previous observations (Motoba et al. 2009; Liu et al. 2015). We do observe a two-step development with weak poleward moving arcs, which after a few minutes stop their poleward movement and increase substantially in intensity. However, we do not observe a difference in the red and green channel in terms of behavior, except for the added poleward arc of the green emission channel.

A sudden brightening of the aurora in response to the IP shock is commonly observed on the dayside within a few hours of LT. The initial brightening is known to immediately propagate to the midnight sector, occupying most of the oval in ~20 min. In contrast to this auroral transient, a sudden brightening of auroral patches with lifetimes of 5–6 min in the midday sub-auroral zone detached from the oval is observed within 1 min of the SC (Liou et al. 2003). This auroral transient is associated with the precipitation of preexisting trapped central plasma sheet particles caused by magnetospheric compression. The reason for the midday sub-auroral patch being separated from the oval is not understood. We do not think that our MSP observations could be interpreted as a manifestation of the short-lived midday sub-auroral patch, because the Svalbard MSP is located at a latitude that would be too high.

Solar wind changes are believed to externally trigger a substorm (e.g., McPherron et al. 1986; Liou et al. 2003), though it remains a controversial issue whether the substorm triggering is caused by the sudden IMF changes that occur simultaneously with a pressure increase, or if the compression itself has a potential to trigger a substorm. In addition, the magnetospheric compression and inward (anti-sunward) displacement of magnetospheric plasma is to be accompanied by an induction electric field, $E_\lambda \sim \partial B_z/\partial t$. Keika et al. (2009) proposed that the inductive downward electric field on the SC compressional front propagating from the dayside magnetopause is a probable candidate for triggering a substorm, but not the disturbances generated by the motion of the flank magnetopause. In the case under examination, the IMF is northward both before and after the SC, which excludes the possibility of substorm triggering associated with a southward IMF. A possible trigger may be transported by a fast compression front from the dayside magnetopause via the magnetosphere or by a disturbance of the solar wind flow around the magnetopause. According to our observations and timing estimates, the inductive downward electric field transported through the magnetosphere to the magnetotail by a fast mode front may be a probable candidate to trigger the substorm. However, whether all substorms are triggered is still a controversial issue, because not all magnetic bays are associated with auroral substorms. Although ~50% of the IP shocks do produce negative magnetic bays at nightside, only less than 10% of the SC causes an auroral breakup (Liou et al. 2003). Therefore, it is likely that the observed magnetic bay at PBK is not associated with the auroral breakup but with enhanced convection due to a sudden compression and should be classified as a "compression bay."

The propagation of the PI from high to low latitudes is often interpreted as an instantaneous transmission of atmospheric TH_o mode along the ionosphere–ground waveguide (Kikuchi and Hashimoto 2016), though some researchers (e.g., Yumoto et al. 1997; Chi et al. 2001) consider this mechanism questionable because of the observed finite time delay between the PI detected at separated sites. Engebretson et al. (1999) revealed dispersive propagation of the PI in early morning hours at speeds decreasing from ~150 to ~50 km/s directly away from a source near the cusp using ground observatories in the Arctic and Antarctic regions. For the event under study, the observed poleward PI propagation pattern contradicts the model of atmospheric TH_o mode near-instantaneous transmission.

Adiabatic compression of the magnetospheric magnetic field, ΔB, results in a particle energization and flux enhancement, ΔJ, that follows as $\Delta J/J \sim \Delta B/B$. According to GOES-13 observations, the sudden enhancement of fluxes of energetic protons is $\Delta J/J = \sim3$ and relativistic electrons is $\Delta J/J = \sim4$, while the magnetic field compression is just $\Delta B/B = \sim0.6$. Therefore, assuming that GOES-13 recorded the enhancement of the energetic particle and magnetic field in the same flux tube, it may be concluded that the detected particle increase is much larger than the limit imposed by the adiabatic betatron mechanism. However, upon the magnetospheric compression, the westward induction electric field produces an Earthward plasma drift. As a result of this additional

Belakhovsky *et al. Earth, Planets and Space* (2017) 69:105

Page 22 of 25

time variation, the betatron acceleration increases by a factor of ~2.5 during the SC (Mal'tsev 1996). In general, the problem of the particle energization by the sudden magnetosphere compression is a separate complicated problem, and a simple interpretation based on the idea of betatron acceleration is insufficient to comply with observations.

A TEC response to IP shock may be considered as a good observational test for the study of the impulsive magnetosphere–ionosphere interaction. To date, a TEC response to the SC has not been well examined and understood. A similar effect was reported by Jayachandran et al. (2011), who found an isolated ~0.6–1.2 TECu pulse produced by a sudden compression of the magnetosphere using CHAIN receivers, but not by the SC. An application of a GPS triangulation technique revealed that the TEC changes propagated with a speed of 3–6 km/s in the anti-sunward direction near noon and ~8 km/s in the sunward direction in the pre-noon lower latitude sector. Simultaneous with the TEC pulse, a small (0.1–0.2 dB) but detectable pulse in absorption was observed. The authors proposed that these TEC changes were seemingly due to electron density enhancement in the F region caused by particle precipitation. In the current examined event, the driver of the SC is different from the event considered in (Jayachandran et al. 2011). The case study of TEC response to IP shock by Jin et al. (2016) suggested that a shock-generated TEC variation is a "duplication" of the shock aurora due to the same mechanism. The core of this mechanism is the generation of electromagnetic VLF waves that cause electron pitch angle scattering into the loss cone and diffuse aurora. This mechanism was proposed to be responsible for the fast anti-sunward propagation of the diffuse auroral-related TEC signal with velocity of ~13 km/s. At the same time, newly established upward field-aligned currents may increase electron precipitation into the ionosphere and cause discrete aurora along the oval poleward boundary. These currents were suggested to be responsible for the random intensification of the auroral-related TEC signal near the poleward oval boundary. However, the idea that the TEC variation is a "duplication" of the shock aurora met with some issues. The observed shock-generated TEC enhancement was a single 2–3-min pulse with a delayed start and peak time, indicating a propagating shock compression, while the diffuse shock aurora lasted ~10–20 min.

During the SC event under examination, the TEC response has been only detected for the MI. The energy of the shock aurora electrons, which are diffuse on closed field lines along the oval and discrete along the oval poleward boundary, is mainly 1–10 keV, although the range may vary from case to case. The corresponding maximum ionization rate occurs at an altitude of 110–160 km. This altitude range corresponds well to the ionospheric density enhancement and plasma heating detected by EISCAT. Therefore, the precipitation of soft electrons caused by the shock compression may be responsible for the TEC pulse. We are not aware of any model that would be capable of estimating the energy spectrum of precipitating electrons from TEC disturbances.

Along with an additional ionization, the modulation of the ionospheric plasma density may be caused by the interaction of an incident MHD pulse with the ionosphere–atmosphere–ground system. The precipitation of energetic electrons and ionization of the lower ionosphere during the SC, responsible for the disturbance recorded by riometers, can influence the bottom E and D layers only. However, a contribution of these layers into TEC is small as compared with that of the F layer. A shear Alfven wave in the magnetosphere does not produce plasma/magnetic field compression, so any compressional effects arise upon interaction of this mode with the anisotropic inhomogeneous ionosphere. The responsible mechanisms may comprise an advection across a steep lateral gradient of the ionospheric plasma, or a plasma compression, $\Delta N/N \sim \Delta B/B$. According to these mechanisms, the lack of N_e response in the F layer evidenced by the EISCAT observations is hard to comprehend. Another possible mechanism is related to field-aligned plasma transport (Belakhovsky et al. 2016). The FAC and flux transported by an Alfven pulse incident onto the ionosphere from the magnetosphere causes an additional accumulation of plasma in regions with strong vertical gradients of the plasma density vertical profile, $N_e(z)$. A significant part of an Alfvenic pulse FAC can be transported by a background suprathermal electron flow into the ionosphere. These electrons do not ionize the ionospheric plasma additionally, so they cannot be detected by riometers, but they can pump the ionospheric TEC. As a result, the plasma density in the bottom ionosphere may increase. The EISCAT-observed increase in N_e at altitudes of 110–180 km during the TEC pulse is in accordance with this mechanism. The TEC modulation due to transient pumping into the lower ionosphere of the field-aligned electron flux transported by an Alfven wave should be related to ground magnetic variations as $\partial_t\{vTEC(t)\} \propto B^{(g)}(t)$. In a realistic ionosphere, several mechanisms may operate simultaneously, so it is hard to discriminate their contribution to the TEC variations. A nearly simultaneous response in riometer, TEC, and EISCAT N_e may be interpreted as a SC-stimulated precipitation of electrons with a wide energy range, from soft (≤keV) to energetic (tens of keV).

While the vast majority of GIC studies focus on severe geomagnetic storms, such space weather phenomenon

Belakhovsky *et al. Earth, Planets and Space* (2017) 69:105

Page 23 of 25

as the SC can also produce very large dB/dt at various latitudes, from an auroral region to the geomagnetic equator (Fiori et al. 2014). Importantly, the SC events are often the precursors to strong geomagnetic storms. Operators of power grid lines take SC as an occurrence of short circuits in the system. The dB/dt levels of 65–120 nT/min were reported during severe magnetic storms at mid-latitudes that led to power equipment failures (Kappenman 2003; Pulkkinen et al. 2012). The dB/dt levels at the equator can be comparable to those in high-latitude regions (Carter et al. 2015). Given previous equipment failures reported for dB/dt levels less than 100 nT/min (Kappenman 2003), the recorded dB/dt of ~180 nT/min (Fig. 14) confirms that IP shock impacts are likely to be a significant factor in power stability problems. For infrastructure not designed to cope with space weather, future studies investigating the direct impact of IP shocks on power grids are strongly encouraged.

Conclusion

The analysis of a SC event recorded simultaneously by various instruments on the ground and in space has shown a surprisingly large variety of associated effects. Though our observations of these effects basically confirm the earlier results and can be principally understood in the framework of existing notions, some features still require additional consideration and modeling.

The conclusions derived from the multi-instrument observations of the magnetosphere–ionosphere effects caused by the IP shock on January 24, 2012, follow. The THEMIS determination of the Mach number of the compressional front from both timing analysis and the jump in the plasma parameters ($M_A \sim 0.2$–0.4) does not support the idea of a shock wave propagation pattern through the magnetosphere. Clear resonant transient Psc5 oscillations are independently generated on the morning and evening flanks, but no signatures of theoretically predicted cavity mode excitation have been found. We could not find a reliable in situ confirmation of the mechanism of PI generation owing to mode conversion at the front of fast mode propagation through the magnetosphere. The observed poleward propagation pattern of the dayside PI contradicts the model of instantaneous atmospheric TH_o mode transmission. Though the SC amplitude is much less than the amplitude of the subsequent substorm magnetic bays, the GIC intensity at the Kola Peninsula power lines caused by the SC is higher than the GIC during the substorm intensifications.

A different TEC response to the SC has been found at latitudes above 60°, with a gradual growth up to ~40% right after the SC in the morning sector and a ~9% positive pulse superposed on a gradual increase in the evening sector. The TEC effect has been compared

in detail with the fine temporal structure of the SC using a comprehensive set of geophysical observations, including magnetometers, riometers, auroral imagers, satellite detectors, and ionospheric radars. To date, the TEC modulation by the SC has not been comprehensively modeled, but on the basis of this multi-instrument information, a validated theory of the magnetosphere–ionosphere response to an IP shock may be constructed. A responsible mechanism of TEC modulation may be related to low-energy electron precipitation and/or field-aligned plasma transport by an Alfven pulse, which provides additional plasma flow into the lower ionosphere.

Author details
[1] Institute of Physics of the Earth, Moscow, Russia. [2] Geophysical Center, Moscow, Russia. [3] Polar Geophysical Institute, Apatity, Russia. [4] UNIS, Longyearbyen, Svalbard, Norway. [5] BCSS, Bergen, Norway. [6] Institute of Cosmophysical Research and Aeronomy, Yakutsk, Russia.

Publisher's Note
Springer Nature remains neutral with regard to jurisdictional claims in published maps and institutional affiliations.

Belakhovsky *et al. Earth, Planets and Space* (2017) 69:105

Page 24 of 25

References

Allan W, Wright AN (1998) Hydromagnetic wave propagation and coupling in a magnetotail waveguide. J Geophys Res 103:2359–2368. doi:10.1029/97JA02874

Araki T (1994) A physical model of the geomagnetic sudden commencement. In: Engebretson MJ, Takahashi K, Scholer M (eds) Solar wind sources of magnetospheric ultra-low-frequency waves, Geophysical monograph series, 81. AGU, Washington, p 183

Belakhovsky V, Pilipenko V, Murr D, Fedorov E, Kozlovsky A (2016) Modulation of the ionosphere by Pc5 waves observed simultaneously by GPS/TEC and EISCAT. Earth Planets Space 68:102. doi:10.1186/s40623-016-0480-7

Béland J, Small K (2004) Space weather effects on power transmission systems: the cases of Hydro-Quebec and Transpower New Zealand Ltd. In: Eaglis IA (ed) Effects of space weather on technology infrastructure. Kluwer, Dordrecht, pp 287–299

Blake JB, Kolasinski WA, Fillius RW, Mullen EG (1992) Injection of electrons and protons with energies of tens of Mev into L < 3 on 24 March 1991. Geophys Res Lett 19:821–824

Carter BA, Yizengaw E, Pradipta R, Halford AJ, Norman R, Zhang K (2015) Interplanetary shocks and the resulting geomagnetically induced currents at the equator. Geophys Res Lett 42:6554–6559. doi:10.1002/2015GL065060

Chi PJ, Russell CT, Raeder J, Zesta E, Yumoto K, Kawano H, Kitamura K, Petrinec SM, Angelopoulos V, Le G, Moldwin MB (2001) Propagation of the preliminary reverse impulse of sudden commencements to low latitudes. J Geophys Res 106:18857–18864. doi:10.1029/2001JA900071

Engebretson MJ, Murr DL, Hughes WJ, Lühr H, Moretto T, Posch JL, Weatherwax AT, Rosenberg TJ, Maclennan CG, Lanzerotti LJ, Marcucci F, Dennis S, Burns G, Bitterly J, Bitterly M (1999) A multipoint determination of the propagation velocity of a sudden commencement across the polar ionosphere. J Geophys Res 104:22433–22451. doi:10.1029/1999JA900237

Fiori RAD, Boteler DH, Gillies DM (2014) Assessment of GIC risk due to geomagnetic sudden commencements and identification of the current systems responsible. Space Weather 12:76–91. doi:10.1002/2013SW000967

Fujita S, Tanaka T, Kikuchi T, Fujimoto K, Hosokawa K, Itonaga M (2003) A numerical simulation of the geomagnetic sudden commencement: 1. Generation of the field-aligned current associated with the preliminary impulse. J Geophys Res 108:1416. doi:10.1029/2002JA009407

Fujita S, Tanaka T, Motoba T (2005) A numerical simulation of the geomagnetic sudden commencement: 3. SC in the magnetosphere-ionosphere compound system. J Geophys Res 110:A11203. doi:10.1029/2005JA011055

Gail WB, Inan US, Helliwell RA, Carpenter DL (1990) Characteristics of wave-particle interactions during sudden commencements 1. Ground-based observation. J Geophys Res 95:119–137

Hartinger M, Angelopoulos V, Moldwin MB, Nishimura Y, Turner DL, Glassmeier K-H, Kivelson MG, Matzka J, Stolle C (2012) Observations of a Pc5 global (cavity/waveguide) mode outside the plasmasphere by THEMIS. J Geophys Res 117:A06202. doi:10.1029/2011JA017266

Holmes JM, Johnsen MG, Deehr CS, Zhou X-Y, Lorentzen DA (2014) Circumpolar ground-based optical measurements of proton and electron shock aurora. J Geophys Res 119:3895–3914. doi:10.1002/2013JA019574

Jayachandran PT, Watson C, Rae IJ, MacDougall JW, Danskin DW, Chadwick R, Kelly TD, Prikryl P, Meziane K, Shiokawa K (2011) High-latitude GPS TEC changes associated with a sudden magnetospheric compression. Geophys Res Lett 38:L23104. doi:10.1029/2011GL050041

Jin Y, Zhou X, Moen JI, Hairston M (2016) The auroral ionosphere TEC response to an interplanetary shock. Geophys Res Lett 43:1810–1818. doi:10.1002/2016GL067766

Kappenman JG (2003) Storm sudden commencement events and the associated geomagnetically induced current risks to ground-based systems at low-latitude and mid-latitude locations. Space Weather 1:1016. doi:10.1029/2003SW000009

Kappenman JG (2006) Great geomagnetic storms and extreme impulsive geomagnetic field disturbance events—an analysis of observational evidence including the great storm of May 1921. Adv Space Res 38:188–199

Keika K, Nakamura R, Baumjohann W, Magnes W, Glassmeier KH, Auster HU, Fornaçon KH, Angelopoulos V, Chi PJ, Fillingim M, Reeves GD, Yumoto K, Lucek EA, Carr C, Dandouras I (2009) Substorm expansion triggered by a sudden impulse front propagating from the dayside magnetopause. J Geophys Res 114:A00C24. doi:10.1029/2008JA013445

Kikuchi T, Hashimoto KK (2016) Transmission of the electric fields to the low latitude ionosphere in the magnetosphere-ionosphere current circuit. Geosci Lett 3:1–11. doi:10.1186/s40562-016-0035-6

Knipp DJ (2015) Synthesis of geomagnetically induced currents: commentary and research. Space Weather 13:727–729. doi:10.1002/2015SW001317

Liou K, Newell PT, Meng CI, Wu CC, Lepping RP (2003) Investigation of external triggering of substorms with polar ultraviolet imager observations. J Geophys Res 108:1119. doi:10.1029/2003JA009984

Liu J, Hu H, Han D, Yang H, Lester M (2015) Simultaneous ground-based optical and SuperDARN observations of the shock aurora at MLT noon. Earth Planets Space 67:120. doi:10.1186/s40623-015-0291-2

Lyons LR (1996) Substorms: fundamental observational features, distinction from other disturbances, and external triggering. J Geophys Res 101:13011–13025. doi:10.1029/95JA01987

Mal'tsev YuP (1996) An electric field induced in the magnetosphere by a sudden impulse. Geomagn Aeron 36:234–237

Mann IR, Milling DK, Rae IJ et al (2008) The upgraded CARISMA magnetometer array in the THEMIS era. Space Sci Rev 141:413–451

McPherron RL, Terasawa T, Nishida A (1986) Solar wind triggering of substorm expansion onset. J Geomagn Geoelectr 38:1089–1108

Motoba T, Kadokura A, Ebihara Y, Frey HU, Weatherwax AT, Sato N (2009) Simultaneous ground-satellite optical observations of postnoon shock aurora in the Southern Hemisphere. J Geophys Res 114:A07209. doi:10.1029/2008JA014007

Nayak C, Tsai L-C, Su S-Y, Galkin IA, Tan ATK, Nofri E, Jamjareegulgarn P (2016) Peculiar features of the low-latitude and midlatitude ionospheric response to the St. Patrick's Day geomagnetic storm of 17 March 2015. J Geophys Res Space Phys. doi:10.1002/2016JA022489

Nishida A (1964) Ionospheric screening effect and storm sudden commencement. J Geophys Res 69:1861–1874. doi:10.1029/JZ069i009p01861

Nishimura Y, Kikuchi T, Ebihara Y, Yoshikawa A, Imajo S, Li W, Utada H (2016) Evolution of the current system during solar wind pressure pulses based on aurora and magnetometer observations. Earth Planets Space 68:144. doi:10.1186/s40623-016-0517-y

Oliveira DM (2017) Magnetohydrodynamic shocks in the interplanetary space: a theoretical review. Braz J Phys 47:81–95

Oliveira DM, Raeder J (2014) Impact angle control of interplanetary shock geoeffectiveness. J Geophys Res 119:8188–8201. doi:10.1002/2014JA020275

Parkhomov VA (1990) Oscillatory structure of the preliminary impulse of the sudden commencement. Geomagn Aeron 30:210–215

Pulkkinen A, Bernabeu E, Eichner J, Beggan C, Thomson AWP (2012) Generation of 100-year geomagnetically induced current scenarios. Space Weather 10:S04003. doi:10.1029/2011SW000750

Saito T, Matsushita S (1967) Geomagnetic pulsations associated with sudden commencements and sudden impulses. Planet Space Sci 15:573–587

Sakharov YaA, Danilin AN, Ostafiychuk RM, Katkalov YuV, Kudryashova NV (2009) Geomagnetically induced currents in the power systems of the Kola Peninsula at solar minimum. In: Proceedings of 8th international symposium on electromagnetic compatibility and electromagnetic ecology, St. Petersburg, pp 237–238

Samsonov AA, Sibeck DG, Imber J (2007) MHD simulation for the interaction of an interplanetary shock with the Earth's magnetosphere. J Geophys Res 112:A12220. doi:10.1029/2007JA012627

Samsonov AA, Sibeck DG, Zolotova NV, Biernat HK, Chen S-H, Rastaetter L, Singer HJ, Baumjohann W (2011) Propagation of a sudden impulse through the magnetosphere initiating magnetospheric Pc5 pulsations. J Geophys Res 116:A10216. doi:10.1029/2011JA016706

Sigernes F, Ivanov Yu, Chernouss S, Trondsen T, Roldugin A, Fedorenko Yu, Kozelov B, Kirillov A, Kornilov I, Safargaleev V, Holmen S, Dyrland M, Lorentzen D, Baddeley L (2012) Hyperspectral all-sky imaging of auroras. Opt Express 20:27650–27660

Smith EJ, Slavin JA, Zwickl RD, Bame SJ (1986) Shocks and storm sudden commencements. In: Kamide Y, Slavin JA (eds) Solar wind-magnetosphere coupling. Terra Sci, Tokyo, pp 345–365

Spann JF, Brittnacher M, Elsen R, Germany GA, Parks GK (1998) Initial response and complex polar cap structures of the aurora in response to the January 10, 1997 magnetic cloud. Geophys Res Lett 25:2577–2580. doi:10.1029/98GL00647

Sun TR, Wang C, Zhang JJ, Pilipenko VA, Wang Y, Wang JY (2015) The chain response of the magnetospheric and ground magnetic field to interplanetary shocks. J Geophys Res 120:157–165. doi:10.1002/2014JA020754

Belakhovsky *et al. Earth, Planets and Space* (2017) 69:105

Page 25 of 25

Tanskanen EI (2009) A comprehensive high-throughput analysis of substorms observed by IMAGE magnetometer network: years 1993–2003 examined. J Geophys Res 114:A05204. doi:10.1029/2008JA013682

Viljanen A (2011) European project to improve models of geomagnetically induced currents. Space Weather 9:S07007. doi:10.1029/2011SW000680

Vorobiev VG, Belakhovsky VB, Yagodkina OI, Roldugin VK, Hairston MR (2008) Features of morning-time auroras during SC. Geomagn Aeron 48:154–164

Watson C, Jayachandran PT, Singer HJ, Redmon RJ, Danskin D (2015) Large-amplitude GPS TEC variations associated with Pc5–6 magnetic field variations observed on the ground and at geosynchronous orbit. J Geophys Res Space Phys 120:7798–7821. doi:10.1002/2015JA021517

Yumoto K, Takahashi K, Ogawa T, Watanabe T (1989) SC- and SI-associated ULF and HF Doppler oscillations during the great magnetic storm of February 1986. J. Geomag. Geoelectr. 41:871–878

Yumoto K, Isono A, Shiokawa K, Matsuoka H, Tanaka Y, Menk FW, Fraser BJ (1994) Global cavity mode-like and localized field-line Pc3–4 oscillations stimulated by interplanetary impulses (Si/Sc): initial results from the 210° MM magnetic observations. In: Solar wind sources of magnetospheric ULF waves. AGU, Washington, pp 335–344

Yumoto K, Pilipenko V, Fedorov E, Kurneva N, De Lauretis M (1997) Magnetospheric ULF wave phenomena stimulated by SSC. J Geomagn Geoelectr 49:1179–1195

Zhang JJ, Wang C, Sun TR, Liu CM, Wang KR (2015) GIC due to storm sudden commencement in low-latitude high-voltage power network in China: observation and simulation. Space Weather 13:643–655. doi:10.1002/2015SW001263

Zhou X-Y, Strangeway RJ, Anderson PC, Sibeck DG, Tsurutani BT, Haerendel G, Frey HU, Arballo JK (2003) Shock aurora: FAST and DMSP observation. J Geophys Res 108:8019. doi:10.1029/2002JA009701